.

Insect antennae: coupling blood pressure with cuticle deformation to control movement

Griffin Donley[1], Yueming Sun[1], Günther Pass[2], Peter H. Adler[3], Charles E. Beard[3], Jeffery Owens[4], and Konstantin G. Kornev[1]

[1]Department of Materials Science and Engineering, Clemson University, Clemson, South Carolina, USA, 29634. E-mail: kkornev@clemson.edu

[2]Department of Evolutionary Biology, University of Vienna, A-1030, Vienna, Austria

[3]Department of Plant and Environmental Sciences, Clemson University, Clemson, South Carolina USA, 29634

[4]Air Force Civil Engineer Center, Tyndall Air Force Base, Florida

Abstract.

Insect antennae are hollow, blood-filled fibers with complex shape. Muscles in the two basal segments control antennal movement, but the rest (flagellum) is muscle-free. The insect can controllably flex, twist, and maneuver its antennae laterally. To explain this behavior, we performed a comparative study of structural and tensile properties of the antennae of *Periplaneta americana* (American cockroach), *Manduca sexta* (Carolina hawkmoth), and *Vanessa cardui* (painted lady butterfly). These antennae demonstrate a range of distinguishable tensile properties, responding either as brittle or strain-adaptive fibers that stiffen when stretched. Scanning electron microscopy and high-speed imaging of antennal breakup during stretching revealed complex coupling of blood pressure and cuticle deformation in antennae. A generalized Lamé theory of solid mechanics was developed to include the force-driven deformation of blood-filled antennal tubes. We validated the theory against experiments with artificial antennae with no adjustable parameters. Blood pressure increased when the insect inflated its antennae or decreased below ambient pressure when an external tensile load was applied to the antenna. The pressure–cuticle coupling can be controlled through changes of the blood volume in the antennal lumen. In insects that do not fill the antennal lumen with blood, this blood pressure control is lacking, and the antennae react only by muscular activation. We suggest that the principles we have discovered for insect antennae apply to other appendages that share a leg-derived ancestry. Our work offers promising new applications for multifunctional fiber-based microfluidics that could transport fluids and be manipulated by the same fluid on demand.

1. Introduction

The paired antennae of insects are highly modified appendages bearing complex sensory organs with various modalities [1-5]. Many antennal sensilla are chemoreceptors, although various mechanoreceptors can perceive a wide range of stimuli, such as touch, air movements, airborne sounds, and electric fields. Thermoreceptors and hygroreceptors can also be present. As multifunctional fibers, the antennae quickly respond to chemicals and minute physical forces, for example, to control flight [6-9], maneuver and avoid obstacles [10-15], hear [16, 17], locate mates and engage in combat [18].

Although behavioral, functional, and structural features of antennae have been documented for a number of insects [5, 19], to the best of our knowledge, their fiber-shape-specific materials characteristics have never been reported. Mechanical properties of antennal fibers are typically extracted implicitly either by modeling the applied forces and torques or by assuming constitutive law for the stress-strain relations of cuticular materials [9, 11, 13, 20-22]. Further developments in insect biology and engineering applications are hindered by the lack of knowledge of mechanical properties of these complex fibers and their structural relations that link to biological performance.

The antennae of adult insects, sensu stricto, vary in shape, but the fundamental structure is consistent[1, 23]. That is, there are three main segments: scape, pedicel, and flagellum (Fig. 1). Articulation of the scape with the head capsule allows antennal movement in various directions, whereas articulation between the scape and pedicel allows for movement only in the vertical plane [5-7, 9, 12, 15, 19, 24, 25].

The flagellum often consists of rigid cuticular rings (i.e., flagellomeres) connected by thin, weakly sclerotized, flexible membranous cuticle[1]. The size and shape of flagellomeres often change along the length of the antenna. Thus, the two joints, together with actuation of associated muscles, are the basis for the mechanical movement of antennae.

From an engineering standpoint what makes the insect antenna an attractive fiber is that muscles do not extend into the flagellum. Yet, insects can manipulate the flagellum by flexing and looping it. For example, when grooming the antenna, some insects can fold it on itself [26], or when maneuvering at high speed, some insects actively bend and flex their antennae [10], or when fighting for females, some male long-horned beetles (Cerambycidae) lash one another with their antennae [18].

This robust manipulation of the muscle-free flagellar fiber is enigmatic. Materials properties of the antennal flagellum have mostly been related to its necklace-like structure [11, 13, 21, 22, 27], and its flexibility has been assigned to the necklace-like arrangement of flagellomeres (rigid rings of the necklace) bridged by membranes working like springs, which allows the stiffer cuticle to bend more readily [7, 13, 21, 22, 24, 27]. The size distribution of flagellomeres has been considered key to understanding the structural properties of this fiber [11, 13, 22].

Although no muscles are in the flagellum, other components run the inner length of the antenna: nerves, an antennal vessel, and tracheae (Fig. 1c). The antennal vessel is a thin conduit connected to a pulsatile organ [28-34] in the head near the antennal base. This so-called antennal heart drives blood through the vessel to the tip of the antenna, where it pours out into the voluminous antennal hemocoel and then flows back to the head.

We hypothesize that the looping, or flexing, of the antennal flagellum can be controlled by blood pressure that, in turn, is controlled by the antennal pulsatile organ and/or by pressure conditions in the region where the antennal hemocoel merges with that of the head capsule. For example, by increasing blood pressure, an insect should be able to extend its antenna. At the same time, the blood might help bear the tensile load and, therefore, less tensile stress would act on the antenna. To examine this hypothesis, we evaluate the effect of blood pressure on the tensile properties of antennae. A comparative analysis of the antennal behavior of adult American cockroaches (*Periplaneta americana*), painted lady butterflies (*Vanessa cardui*), and Carolina hawkmoths (*Manduca sexta*) allows us to evaluate how the shape of the antennal lumen and blood content influence the tensile behavior of this natural fiber.

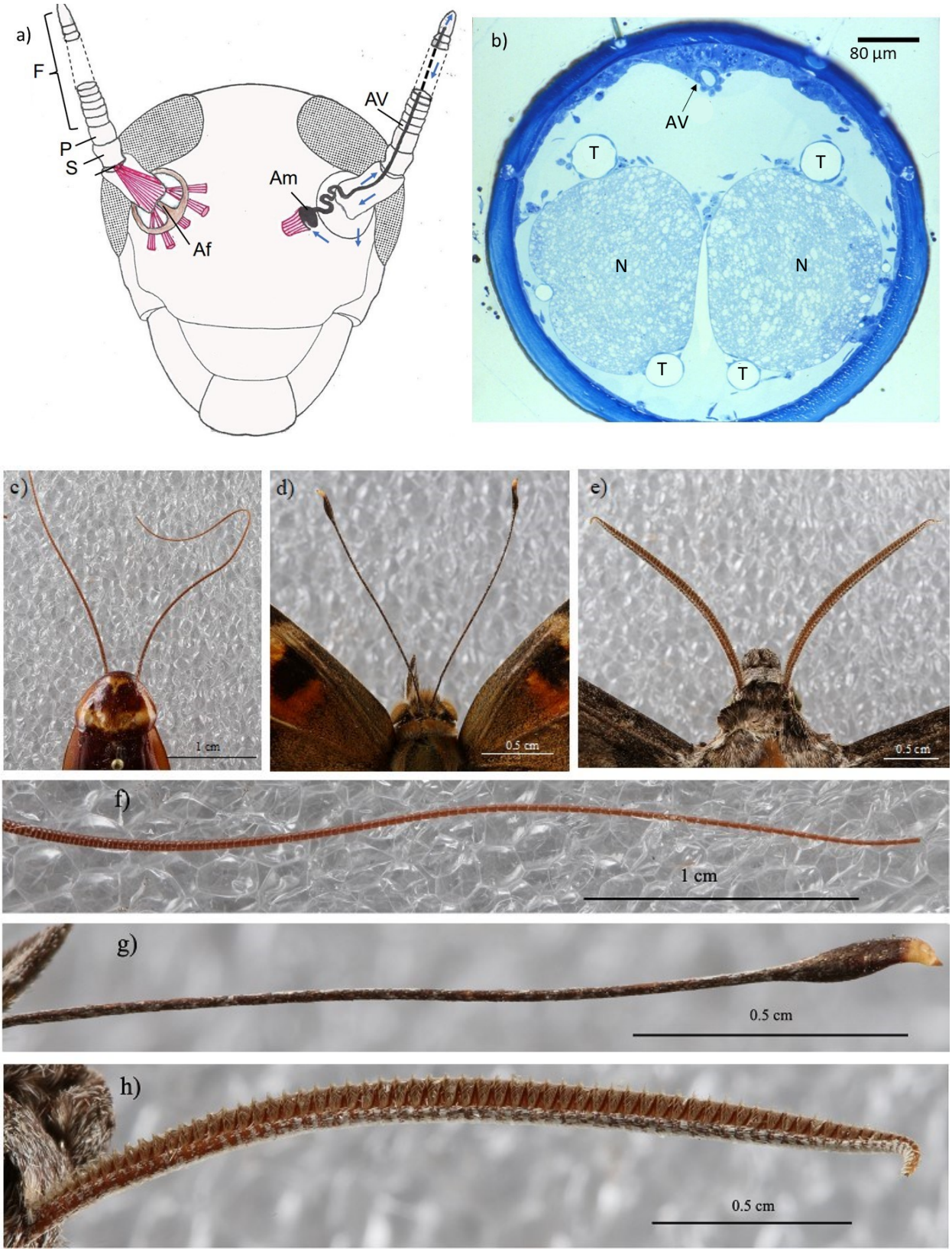
a)
F
P
S
Am
AV
Af
b)
80 µm
AV
T
T
N
N
T
T
c)
1 cm
d)
0.5 cm
e)
0.5 cm
f)
1 cm
g)
0.5 cm
h)
0.5 cm

Figure 1. a) Schematic of the insect head (frontal view). Each antenna consists of three basic components: scape (S), pedicel (P), and flagellum (F). The left side shows the movement apparatus of the antenna. The antennifer (Af), a cuticular process of the sclerotized antennal ring that forms the articulation point (Am) of the scape, allows the antenna to move freely in all directions; between the scape and pedicel is a hinge joint allowing only up and down movements. The flagellum cannot be actively moved by muscles. The right side shows the circulatory organ associated with each antenna. Close to the antennal base is a pulsatile ampulla (Am) that is connected to the antennal vessel (AV) shown as a solid line that runs along the antenna. Blood enters the ampulla through a slit-shaped ostium and flows to the tip, where it pours out into the lumen of the antenna and flows back into the head capsule. Blue arrows indicate blood flow. b) Semithin cross-section of a flagellomere of *Periplaneta americana* close to its base. Two massive nerves (N) are purely sensitive and originate from the numerous sensory neurons on the antennae; four tracheae (T) and an antennal vessel (AV) also occupy the lumen. c–e) Insect heads with intact antennae: c) American cockroach, d) painted lady butterfly, e) Carolina hawkmoth. f–h) Antennae: f) American cockroach (*P. americana*), g) painted lady butterfly (*Vanessa cardui*), and h) Carolina hawkmoth (*Manduca sexta*).

2. Materials and Methods

2.1 Insect Rearing

American cockroaches were obtained from a long-standing colony at Clemson University. They were raised from eggs to adults at 24°C, 70% relative humidity, and a 14:10 hour light/dark cycle in 4-liter glass jars with screen lids, dog food, and a water dish. Painted lady butterflies and Carolina hawkmoths were obtained as eggs and young larvae from Carolina Biological Supply (Burlington, NC) and Great Lakes Hornworms (Bruce Township, MI), respectively, and raised in continuous low light at room temperature on prepared media from these companies. Larvae of the butterflies were held with their diet in plastic mosquito emergence containers (BioQuip Products, Rancho Dominguez, CA), whereas those of hawkmoths were held, with their diet, in 1-liter glass jars with screen lids. Butterfly larvae were allowed to pupate in their containers, whereas hawkmoth larvae, once they entered a non-feeding, wandering stage, were transferred to 1-liter plastic beakers with shredded-paper bedding and allowed to pupate. Pupae of both species were then placed in collapsible, nylon-mesh insect cages for adult emergence at > 60% humidity and a 12:12 hour light/dark cycle. Butterfly pupae were pinned to the cages through the non-living, posterior end of the pupa, whereas hawkmoth pupae were held in the paper-filled beakers. Once adults emerged, they were fed *ad libitum* on sugar water, butterflies from saturated paper towels and hawkmoths from tubes with 15 ml of fluid.

2.2 Semithin Sections

Antennae of the American cockroach were fixed in alcoholic Bouin's solution (Dubosq-Brasil mixture), dehydrated in acetone and embedded in Agar low-viscosity resin (Agar Scientific Ltd., Essex, UK) under vacuum impregnation. The sections (1 µm thick) were cut with an ultramicrotome and stained with a mixture of methylene blue (1%) and azure II (1%) in an aqueous borax (1%) solution to produce Fig. 1b (n = 1).

2.3 Scanning electron microscopy (SEM)

All antennae were cut from living insects less than 12 hours before SEM observation. Seven samples, each 300–500 microns in length, from each species were analyzed. Specimens were attached to an SEM mount with carbon-graphite adhesive tape; they were not coated with a heavy metal (i.e., gold or platinum). A Hitachi SU5000 VP-SEM was used to image the samples, with the BSE detector at an accelerating voltage of 15 kV or 20 kV in low-vacuum mode at 50–70 Pa.

2.4 Antennal removal

Adult American cockroaches (> 5 months old) and painted ladies and hawkmoths (both < 2 weeks old) were used in experiments. One antenna from each of 10 specimens of each species was removed for MicroTensile analysis. Each antenna was cut with microscissors between the pedicel and scape. The date, insect age, temperature, humidity, and time were recorded for each antennal removal (**Supplementary Material**, Table S1).

2.5 MicroTensile testing of antennae

A MicroTensile Tester 2000 (Rheometric Scientific, US) was used for tensile testing. Once the antenna was cut, it was mounted in a holder to aid in the loading process to the MicroTensile Tester. Two Dia-Stron brass crimps (Dia-Stron, UK) were taped to the ends of a block "C" mount. The ends of the brass crimps were attached along the inner edge of the "C" so that 1 cm of space was between them to accommodate the antenna. The antenna was placed in crimps so that its midpoint was midway between the crimps. The ends of the crimps were clamped to fix, but not fracture, the antenna in place. The entire holder was placed in the loading cell of the MicroTensile Tester 2000 and fixed in the two clamps. The section of the "C" paper holder that was parallel to the antenna was cut so the antenna was the only connection between the two clamps (Fig. 2). The loading cell of the MicroTensile 2000 with the antenna was housed under an Olympus MVX10 microscope with an attached Point Grey high-speed camera. A small length of copper wire of known diameter was placed in the video frame as a reference distance for future measurements. Tensile testing was conducted on the antenna and the data were acquired with the Minimat software and then transferred to Microsoft Excel for analysis. For all three types of antennae, the tests were conducted at a clamp speed of 2 mm/min. All tensile testing was conducted at 22°C with humidity ranging from 22% to 77%.

Once the test was completed, the end of the broken antenna was analyzed in cross section, using a Huvitz light microscope (Model HR3-TRF-P). The flagellomere of the antenna that broke during testing was cut off and placed upright on a glass slide. The thickness h of the cockroach's and butterfly's cuticular shell was measured from the outer to inner edge of the cuticular ring and the external diameter d of the flagellomere was measured from the side, measuring from one outer edge of the flagellomere to the other edge. These parameters were used to calculate the area of the flagellomere cross section as $A = \pi(\frac{d^2}{4} - \left(\frac{d}{2} - h\right)^2)$. This area was used to evaluate the tensile stress acting on the flagellomere and was measured ~1/3 of the distance from the distal end of the cockroach antenna and ~1/10 from the distal end of the butterfly antenna. For the hawkmoth antenna, only the ring connecting one flagellomere to another supports the tensile stress. Its thickness h and contour length c were measured using ImageJ. These parameters were used to calculate the area of the cross section as $A = ch$ and was measured at ~15% of the distance from the distal end of the antenna. Measurements are given in **Supplementary material**. Each set of stress-strain data was normalized to the breaking strength of the antenna and its corresponding

strain at the break. Average values and standard deviations in Fig. 3b were determined from the maximum breaking strength, the amount of extension at which fracture occurred, and the diameter of all samples tested for a particular antenna or fiber. For the cockroach, hawkmoth, and butterfly (high humidity regime), 10 antennae each were used.

2.6 Measurements of Poisson's ratio

To measure Poisson's ratio, a distinct defect, specific sensillum, or well-defined membrane connection (e.g., Fig. 9 and **Supplementary material**) was used as the location at which the diameter d_0 of the flagellomere was taken at the first moment of time. To measure the flagellomere diameter d as a function of extension $\Delta L/L$, these landmarks were traced until the last frame before the antenna fractured. Changes in flagellomere diameter could be used to find the axial strain as $\varepsilon_{||} = \Delta L/L$, as measured by the MicroTensile tester. The circumferential strain $\varepsilon_{\perp}$ | at two different points – landmarks A ($\varepsilon_{\perp}^{A}$) and B ($\varepsilon_{\perp}^{B}$) – that were easily recognizable and traceable, were determined for each antenna and averaged together $\varepsilon_{\perp}^{i} = \frac{(\varepsilon_{\perp}^{A} + \varepsilon_{\perp}^{B})}{2}$ to get the circumferential strain for the i-th antenna. The average Poisson ratio was then calculated as:

$$\nu_i = -\frac{\varepsilon_{\perp}^{i}}{\varepsilon_{||}^{i}}, \text{ where, } i = 1 \ldots n;$$

$$\nu_{avg} = \frac{(\nu_1 + \nu_2 + \nu_3 + \ldots + \nu_n)}{n}. \quad (1)$$

This process was completed for 5 cockroaches, 5 butterflies, and 5 hawkmoths (1 antenna per individual). The values for each species were averaged to determine the average Poisson's ratio for each species. Poisson's ratios were also measured at the membranes connecting 2 adjacent flagellomeres, as discussed in **Supplementary information**. Due to the non-circular shape of the antenna of *Manduca sexta*, the height (H) of the flagellomere was measured as opposed to the diameter to calculate Poisson's ratio of the flagellomere. The height was considered the distance from the dorsal to the ventral side of the antenna. The diameters of the circular membranes connecting two flagellomeres were used to calculate Poisson's ratio of these membranes.

2.7 Tensile testing of plastic tubes

Plastic tubes (Polypropylene, First Mark®) were tensile tested on the Instron machine (Model 1125) to understand how being filled with a liquid influences the mechanical properties of such a complex fiber. Empty tubes (n = 11) and tubes filled with water (n = 11) were tested and compared. A single tube was cut in half and used as a reference empty straw. The other half was filled with water. To maintain cylindrical shape of the straw, a machine screw (5 mm diameter, 0.8 mm per thread, and 16 mm length) was inserted into the ends of the straw so that the Instron clamps pressed down on this harder material, but not deforming the straw. Hot glue was added to the open end of the tube, and the screw was inserted before the glue hardened. More hot glue was added at the boundary of the screw and end of the tube to form a tight seal. For the water-filled samples, water was added to the open end of the straw, filling it completely. For both filled and empty tubes, the

same process was done to insert another screw on the other end. After drying, the tube was ensured to have no leaks in the hot-glue seal.

2.8 Statistical Analysis

MicroTensile testing was conducted on n = 10 antennae for each species. In addition to the 10 butterfly antennae tested at high humidity, an additional 4 were tested at low humidity, one of which was an extreme outlier and was not used in data representation. For each fiber tested, 3 samples were used.

The curve describing the average values of the experimental data points was determined by using the "polyfit" function within MATLAB to calculate a linear curve of best fit using all available data points up to 2% strain values for n = 11 samples. The error bars at each strain value (0.5%, 1.0%, 1.5%, and 2.0%) used available data points within $\pm 1\%$ to determine the standard deviation at that point. Thus, the error bars represent the spreading of data points seen as strain increases. The average values and standard deviations of all parameters regarding tensile testing of straws (Table 3) were determined from n = 11 samples.

3. Results

3.1 Structural features of antennae

Antennae of the cockroach, butterfly, and hawkmoth all have the basic components (scape, pedicel, and flagellum) (Fig. 1), but the structure and accompanying features are different in each species. Flagellomeres of cockroaches are almost cylindrical with a small taper toward the free end of the antenna (Fig. 2a). The flagellomere is covered with a dense forest of sensilla that, in the resting position, are tilted toward the surface. Each sensillum is secured in a socket so that it emanates from a pit bordered by a thin ring rising above the surface of a flagellomere. Adjacent flagellomeres are connected by membrane.

The butterfly antenna consists of long, slender flagellomeres (Fig. 2b) connected by membrane. Scales are distributed along the entire length but could be easily brushed off, indicating a weaker point of attachment than the sensilla on the cockroach antenna. Towards the tip of the antenna, an elliptical club formed as the flagellomeres increase and then decrease in diameter (Fig. 2f).

The structure of the antenna of the moth is more complex. The two sides of the antenna in males differ [35]; the dorsal side is covered with scales similar to those of the butterfly. These are short hair-like features, easily brushed off. The ventral side of the antenna of males (but not females) has long hairs (fasciculate setae) that are well attached to the flagellomere. The antenna is pectinate (i.e., comblike) (Fig. 2k).

The main differences among the three species are in the internal structure of the flagellomeres.

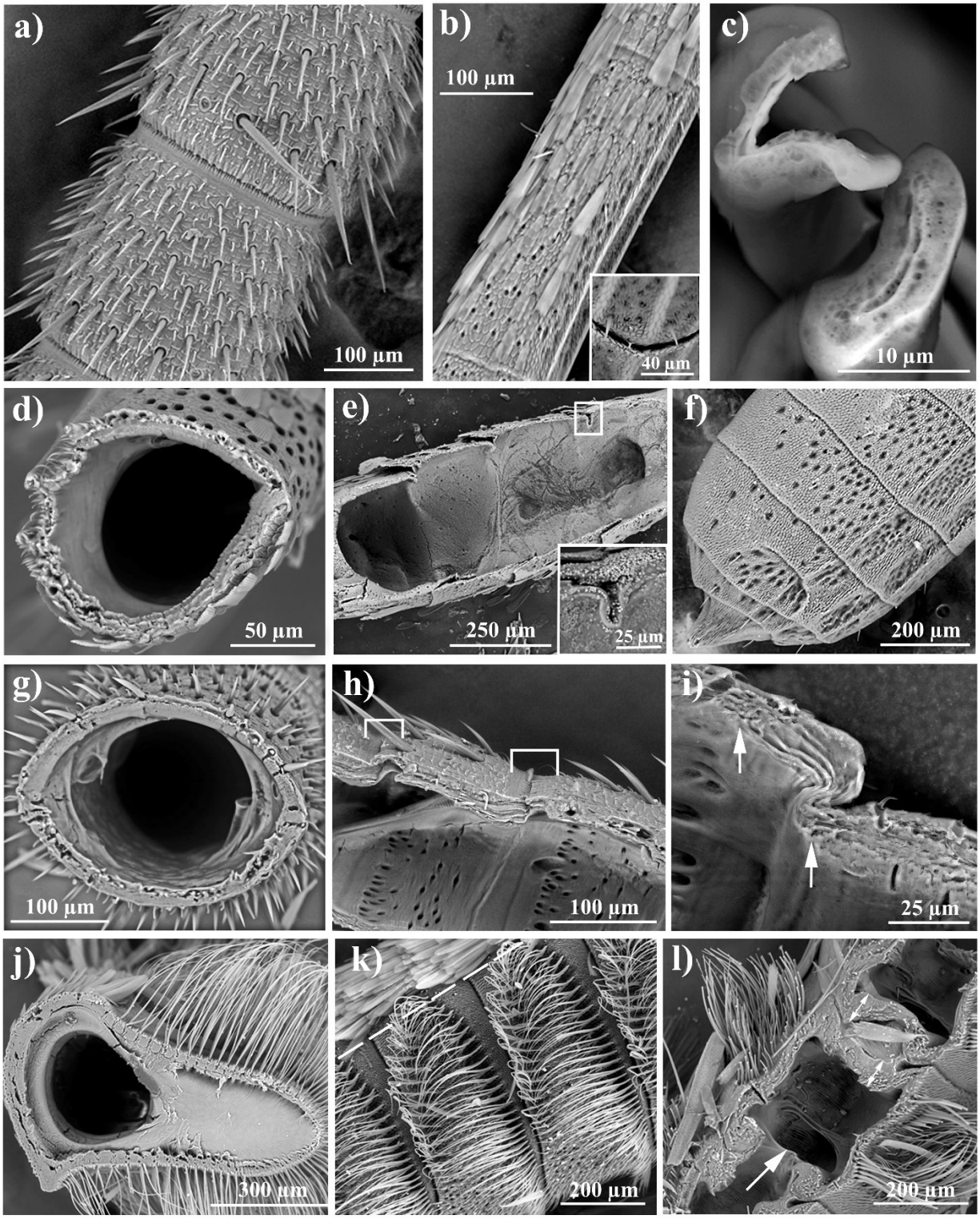

Figure 2. SEM micrographs of antennal structure. a) *Periplaneta americana*. Sensilla are tilted with respect to the antennal axis. b) Flagellomeres of *Vanessa cardui* in the middle of the antenna where diameter does not change significantly and is nearly cylindrical. The flagellomeres are long compared to those of *P.*

americana. Adjacent flagellomeres form a gap, shown in the inset. c) For comparison, a cotton fiber has no flagellomere-like partitioning along its length. It is a tube with a hollow crescent core. Its mechanical properties differ from those of the antennae of *P. americana* and *V. cardui* but are somewhat similar to those of *Manduca sexta*. d) Antenna of *V. cardui* broken during tensile test. The crack nucleated at the membrane and propagated circumferentially, forming this cross-section. e) Flagellomeres of the antennal club of *V. cardui* cut along the antennal axis, showing folds in the inner membrane; the folded membrane is shown in the inset. f) Proximal portion of antennal club of *V. cardui*. g) Antenna of *P. americana* broken during tensile test. h) A fracture running along the antennal axis of *P. americana* shows membrane (bracketed) connecting flagellomeres. i) Enlarged view of membrane between two flagellomeres of *P. americana*; extent of membrane indicated by arrows). j) Antennal cross-section of *M. sexta*. The pectination can be seen as the extension to the right. k) The ventral side of the antenna of *M. sexta* in males is covered with long, hair-like sensilla; the dorsal side (not shown) has short sensilla. The dashed line shows the direction of a cut separating the pectinations in l) from the dorsum of this antenna. l) Longitudinal section of flagellomeres of *M. sexta*, viewed from the ventral side perpendicular to the dashed line in k). The arrow points to a hole connecting the pectination with the antennal lumen. The pectination forms a chamber for blood and houses nerve bundles connected to sensilla. Adjacent pectination chambers are separated by arc-like cuticular walls; two walls are marked by double arrows drawn through their thickness.

Periplaneta americana

Membrane connects flagellomeres to one another, but each flagellomere itself is a hard cuticular shell with a circular cross-section. By crushing the antenna to slightly flatten it and cutting it in half along the antennal length, the profile of the cuticular wall can be observed (Fig. 2h, i). The cuticle of the membranes and flagellomeres are continuous along the length of the antenna. Hence, stress can be transferred when the antenna is deformed.

Vanessa cardui

The flagellomeres are elliptical in cross-section at the club (Fig. 2f) but are more circular in cross-section at the middle of the antenna (Fig. 2g). As with the cockroach antennae, those of *V. cardui* also have membrane connecting the hard cuticular flagellomeres to one another.

In the resting state, flagellomeres are assembled as a column of coffee cups, with one flagellomere resting within another. This arrangement was seen most clearly in the club; when two adjacent flagellomeres meet, their conical shells firmly fit one within the other. Casual observation would not indicate that these flagellomeres are connected; by viewing the antenna at an angle, a slight gap separating flagellomeres was visible (Fig. 2b inset).

A folded membrane is seen by cutting the antenna with a razor blade at an angle along its axis (Fig. 2e). This membrane folds inward toward the center of the antennal lumen and is continuous with adjacent flagellomeres.

Manduca sexta

In cross section, the antenna of *M. sexta* has a rounded dorsal side and elongated ventral pectination (Fig. 2j). During tensile testing, the ventral pectination of the flagellomeres separated after extension. Each flagellomere connects to another by a cuticular ring that is a continuation of the membrane on the dorsal side of the antenna. Each extension of the pectination has a chamber

(Fig. 2l). A hole in the extension enables nerve bundles from the lumen to connect with the long sensilla. Blood could circulate through the antennal lumen and fill the chamber via this hole.

3.2. Tensile properties of insect antennae

The stress acting over the cuticular wall was defined as the applied force F measured by the instrument, distributed per cross-sectional area A of the antennal wall,

$$\sigma_{||} = \frac{F}{A}, \qquad \varepsilon_{||} = \Delta L/L \tag{2}$$

In eq. (2), the strain $\varepsilon_{||}$ was defined as the antennal extension ΔL divided by the initial length L of the antennal piece fully straightened but not yet deformed, $\varepsilon_{||} = \Delta L/L$ (Fig. 3b).

a)

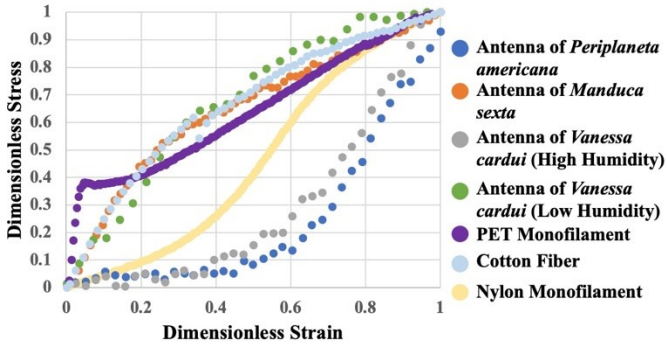

b)

Sample Type	Average Diameter (μm)	Max Load (MPa)	Extension at Break (mm)
Periplaneta americana	226±23	6.43±2.31	0.19±0.06
Vanessa cardui (high humidity)	686±89	1.21±0.52	0.42±0.15
Vanessa cardui (low humidity)	612±247	3.8±1.2	0.66±.54
Manduca sexta	369±48*	4.12±1.69	1.04±0.42
PET Monofilament	92±1	822.4±28.5	24.7±2.7
Cotton Fiber	250±5	109.7±19.0	9.4±1.7
Nylon Monofilament	280±1	1065.9±22.0	9.6±1.5

Figure 3. a) Normalized load-extension curves of insect antennae compared with cotton and synthetic fibers. The stress is normalized as $\sigma = \sigma_{||}/\sigma_{||}^{break}$ and the strain is normalized as $\varepsilon = \varepsilon_{||}/\varepsilon_{||}^{break}$. b) Comparison of tensile properties of insect antennae and synthetic and natural fibers. Average antennal diameter for each species (n = 10 antennae/species) was calculated by measuring the diameters at the point of fracture and then averaging the values for each species. Explanation of "diameter" is given in the section for *Manduca sexta* below. The breaking strain can be calculated by dividing the last column by 10 mm (as the initial length of the specimens was 10 mm).

Periplaneta americana

The tensile stresses of the antennae were measured on the megapascal scale, suggesting that it takes little force to break them (Fig. 3b). Figure 3a shows the normalized stress-strain curve calculated using the breaking strength, $\sigma_{||}^{break}$, the maximum stress experienced by the antennae before fracture. This breaking strength was typically within the range of $5\,MPa < \sigma_{||}^{break} < 9\,MPa$, with the corresponding strain at break $\varepsilon_{||}^{break}$ in the range of $1.5\% < \varepsilon_{||}^{break} < 3\%$.

Vanessa cardui

Testing was conducted at different humidities, from 35% to 66%, and at an average temperature of 22℃ (Table S1 in **Supplementary material**). At higher relative humidity (55–60%), antennae from n = 10 butterflies were tested. These 10 antennae showed J-type stress-strain curves similar to those of *P. americana*. At lower relative humidity (35%), n = 4 butterflies were tested and these 4 antennae showed a more Hookean behavior with a linear increase of stress at small strains.

At the higher humidity range, the breaking strength, $\sigma_{||}^{break}$, of these antennae ranged from 0.75 MPa to 1.5 MPa, with strains ranging within 2.5% < $\varepsilon_{||}^{break} < 6\%$, with one exception that fractured at $\sigma_{||}^{break} = 2.5$ MPa and $\varepsilon_{||}^{break} = 3\%$ strain.

At the lower humidity range, the breaking strength, $\sigma_{||}^{break}$, of these antennae ranged from 3.1 MPa to 4.84 MPa, with strains ranging within 3% < $\varepsilon_{||}^{break} < 4.6\%$. One outlier had a breaking strength of 2.5 MPa and a strain of 14.7%.

Manduca sexta

Testing was conducted at humidities from 33% to 37% and an average temperature of 22℃ (Table S1 in **Supplementary material).** As follows from the analysis of flagellomere morphology, the extensions of the pectination were separated one from the other and hence did not transfer the tensile stress. Only the membrane supported the tensile load between flagellomeres.

The mechanical behavior of antennae of *M. sexta* differed from that of *P. americana* and *V. cardui* tested at high humidity. In contrast to the concave J-type stress-strain curves, the stress-strain curves of the hawkmoth were convex (i.e., they curved outward). These antennae also elongated much more before fracture. The breaking strength ranged from 2.2 MPa to 6.0 MPa with strains varying in the range of 9% < $\varepsilon_{||}^{break} < 16\%$. One exceptional sample fractured at 8000 MPa, with a strain at the breaking point of $\varepsilon_{||}^{break} = 21.3\%$. Two additional trials were conducted in the high humidity range (64% and 84%) and resulted in similar stress-strain curves with Hookean behavior at small strains, indicating that humidity does not influence tensile behavior.

All data were collected to show the difference between mechanical behavior of antennae of the three species and some polymeric fibers (Fig. 3a). The stress-strain curves were normalized to the maximum load for each sample and their corresponding extension at break. The polyethylene terephthalate (PET) fiber exhibited a typical stress-strain curve for polymeric fibers, whereas the Nylon fishing line had a curve similar to an elastomer (S-type). The shape of the first section of the Nylon curve was comparable to that of the cockroach and butterfly antennae (J-type), but the actual physical values differed. Although the J-type behavior of these fibers was unique, compared with common polymeric fibers, the deformations and loads that the fibers supported were orders of magnitude different with regards to the maximum breaking strength.

In contrast, the hawkmoth antenna and the butterfly antenna tested at low humidity belonged to a different category of fibers, demonstrating mechanical reaction nearly identical to that of the cotton fiber. Both fibers were hollow, yet their cross-sectional shapes differed and the insect antenna had nerves, antennal vessel, tracheae, and blood in its core.

A J-type unique stress-strain relationship suggests that a material could have almost no resistance, and hence large extensions at small stresses, and then could stiffen at greater extensions.

This relationship is not common in synthetic polymers but is common for biomaterials [36]. The J-type curve, otherwise known as a strain-adaptive curve [37], is typically caused by moving of crosslinks or entanglements or deforming more complex structure of polymer complexes in synthetic polymeric materials. In insects, the cuticular material of antennae is stiff [13, 22, 38] and the stress-strain relation would not be of the J-type. To date, the behavior of segmented cuticular materials in insects has been thought to be dominated by the connecting soft membranes for which the J-type curve shows up when the strain is not less than 20% [39]. Insect antennae, however, break at much lower strains. Therefore, we suggest that the antennal mechanical response is orchestrated by a complex coupling between blood pressure and structural organization of the antenna as a complex shaped shell. The structural organization might include re-orientation of fibers in the soft membranes upon stretching [39].

3.3. Characteristic features of antennal behavior during extension

To understand mechanisms of antennal deformation, we performed a video analysis of antennal behavior during extension. The following features help understand the common mechanisms of load transfer and differences among species associated with individual behavioral and physiological settings:

Periplaneta americana

a. Thread pull after breakup

After the fracture of the membrane between flagellomeres, a thread-like structure, possibly an antennal nerve or trachea, was pulled from inside the flagellomere (Fig. 4; **Supplementary video**). Blood flowed from the surface of this thread back into the broken end of the flagellomere, suggesting that blood plays an important role in distributing the load.

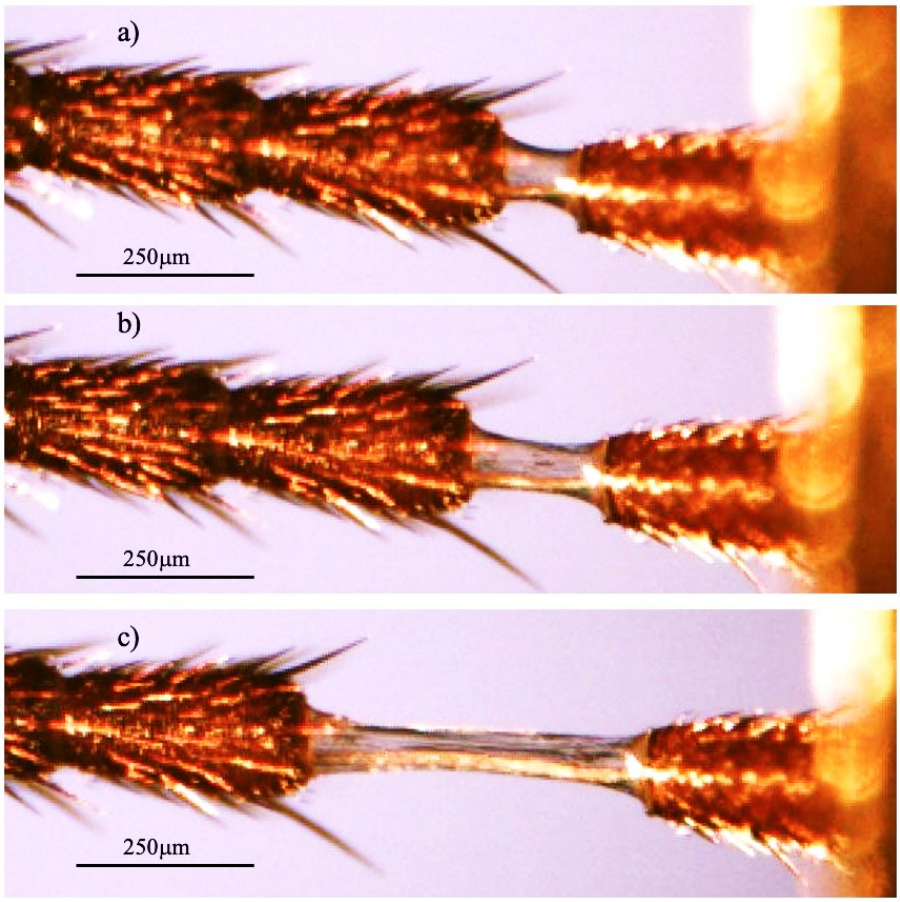

Figure 4. a) Pulling a thread from the flagellum of an American cockroach after t = 6 seconds from antennal fracture. The clamp (shown on the right) moved 0.2 mm from the initial position; b) at t = 8.7 seconds, the clamp moved 0.29 mm; c) at t = 18.45 seconds, the clamp moved 0.615 mm.

b. Unfolding of connecting membranes in *Periplaneta americana* and *Vanessa cardui*

Video analysis of radial deformation of the connecting membranes revealed an unexpected phenomenon further distinguishing *P. americana* and *V. cardui* from *M. sexta*. In *V. cardui*, the free end of the antenna formed a club (Fig. 2f). Filming the behavior of the club during antennal extension, we observed that the edges of the flagellomeres expanded (Fig. 5a–c). At the club, this expansion happened more quickly and to a greater extent compared with flagellomeres closer to the midpoint of the antenna. The same effect was observed at flagellomere edges in the middle of the antenna of *V. cardui* and with connecting membranes of the antenna of *P. americana.* A schematic illustrates the mechanism of opening the cuticular rings caused by tensile deformation of conical flagellomeres and unfolding of the connecting membranes (Fig. 5d). The flagellomeres of *V. cardui* expanded during extension. The structure of this inner membrane might be a contributor. In step one, the membrane was folded in its original position, connecting the end of the more distal flagellomere (left) to the adjacent flagellomere about ¼ of the way from the tip. During stretching, this membrane unfolded, pushing the tip of the flagellomere outward and

appearing to expand it in diameter. We also noted that during stretching of the antenna of *P. americana*, the hair-like sensilla decreased their angle of tilt (Fig. 5e, f).

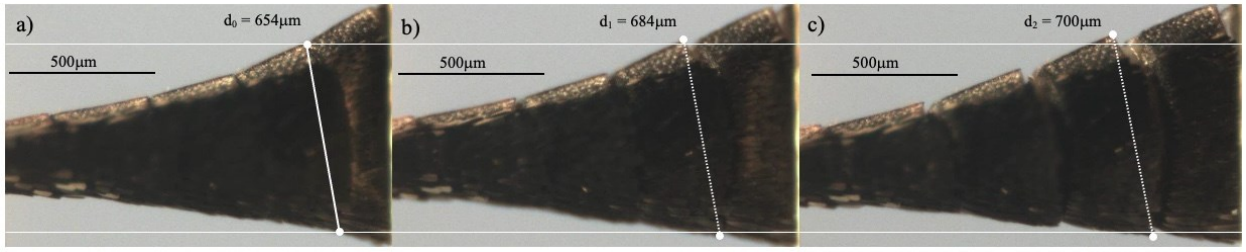

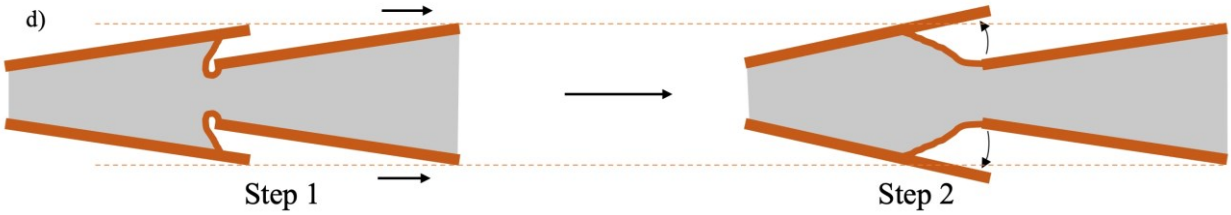

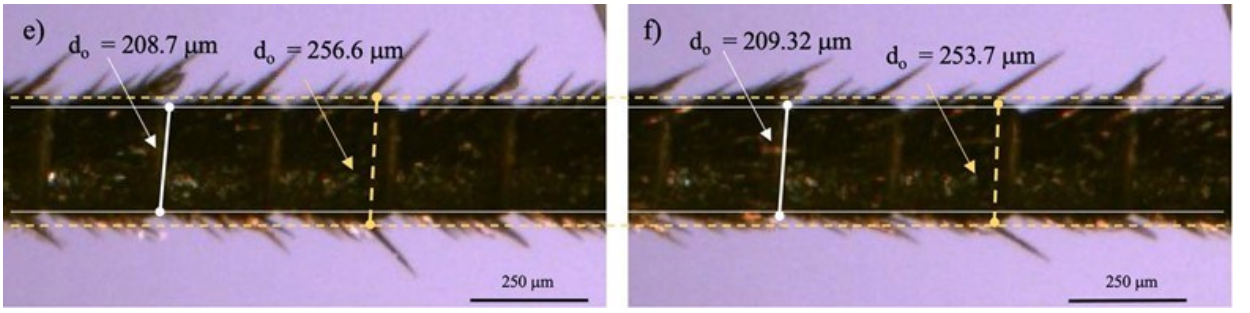

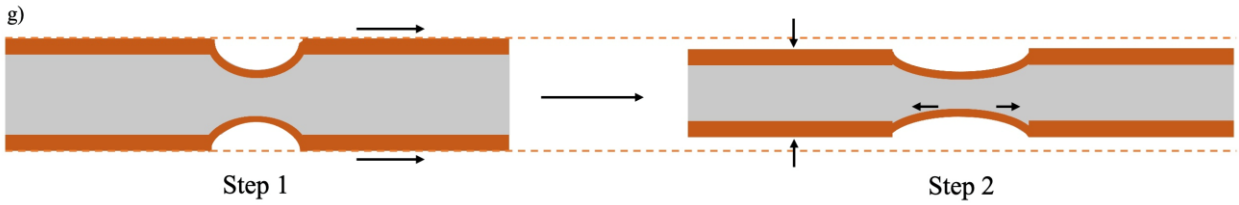

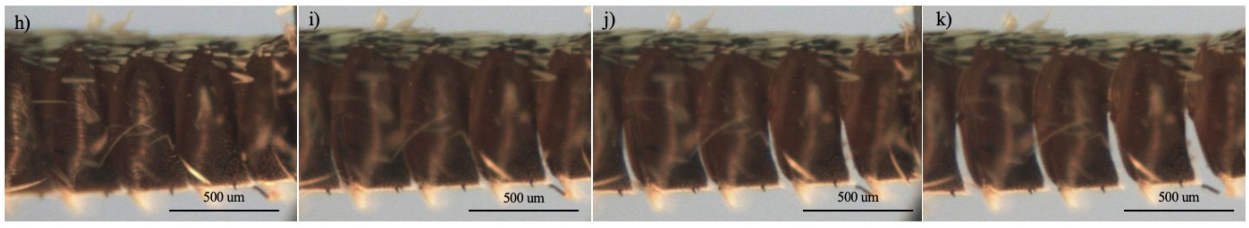

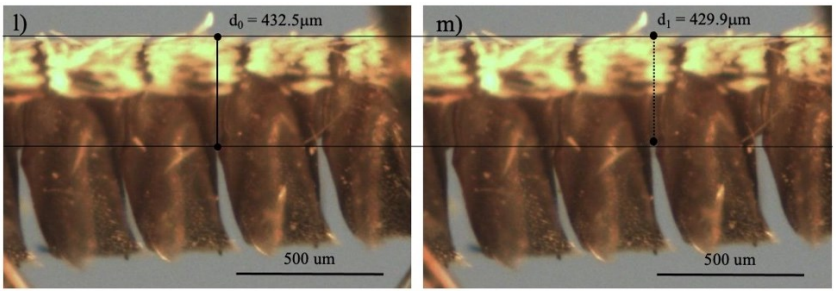

Figure 5. a) The reference state of the antennal club of *Vanessa cardui* at time moment t = 0, with no extension; d = diameter. b) The club after t = 6 s of extension when the right clamp moved 0.2 mm to the right. c) The club after t = 12 s of extension when the right clamp moved 0.4 mm to the right. d) The mechanism of expansion of cuticular rings of flagellomeres of *V. cardui* due to tensile deformation and unfolding of the connecting membrane. The horizontal arrows point toward the moving clamp in the direction of antenna extension. During extension, membrane unfolds and pushes the edge of the flagellomere outward, causing expansion. e) Reference state of the antenna of *Periplaneta americana* at time moment t = 0, with no extension. The dashed line refers to the initial diameter of the flagellomere. f) The antenna after t = 0.74 s of extension when the right clamp moved 0.024 mm to the right. Notice how the diameter of the connection between flagellomere increases whereas the diameter of the flagellomere itself decreases. g) The mechanism of unfolding of the connecting membranes of *P. americana*. The horizontal arrows point toward the moving clamp at the right. Neighboring flagellomeres are shown as solid rectangles and connecting membrane is shown as the solid arc. This membrane naturally bends inward toward the lumen. When the flagellomeres move apart, the membrane flattens and the flagellomeres compress, as shown in step 2. Thus, the apparent diameter of this membrane increases. h) Separation of the ventral extensions of flagellomeres of *Manduca sexta* at t = 0 seconds. i) Separation of the ventral extensions of flagellomeres after t = 10 s when the right clamp moved 0.33 mm to the right. j) Separation of the ventral extensions of flagellomeres after t = 15.03 s when the right clamp moved 0.501 mm to the right. k) Separation of the ventral extensions of flagellomeres after 20 s when the right clamp moved 0.667 mm to the right. l) The antenna of *M. sexta* at time moment t = 18.27 after extension when the right clamp moved 0.61 mm. m) The antenna after t = 24 s of extension when the right clamp moved 0.8 mm to the right.

a. Separation of ventral chambers of flagellomeres on antennae of *Manduca sexta*

Video analysis of stretching of the moth antennae indicated that the flagellomeres were not connected to one another along the entire contour of the cross section. Each flagellomere was connected to the next one by a cuticular ring on the dorsal half of the flagellomere and the ventral extensions were individual chambers that were not directly attached to each other (Fig. 5h–k).

Blood was not seen at the fractured end except once, indicating that the antennal lumen was not completely filled with blood as it was for the cockroach antenna. Based on the diameter and thickness of the membrane connecting flagellomeres after each tensile test, the cross-sectional area in the form of a solid circular ring was used in the calculation of stress.

3.1.Shrinkage/expansion of flagellomeres during antennal extension

The presence of incompressible blood in the antennal core would first manifest as a special radial deformation of the antenna. Assuming that the antennal core is incompressible, one would expect for a cylindrical flagellomere of length l and diameter d to maintain the same volume, $=$

$\pi l d^2/4 = \pi l_0 {d_0}^2/4$, where d_0 and l_0 are the flagellomere diameter and length, respectively, before extension. Therefore, the radial strain

$$\varepsilon_\perp = \frac{d - d_0}{d_0}, \tag{3}$$

and the longitudinal strain

$$\varepsilon_{||} = \frac{l - l_0}{l_0}, \tag{4}$$

should be related as

$$\nu = -\varepsilon_\perp/\varepsilon_{\|} = 1/2. \tag{5}$$

Equation (5) defines Poisson's ratio for the fiber. In the next section, we check relation (5) for antennae of all 3 insects.

Table 1. Poisson's ratio for different insect antennae at flagellomere and membrane. connections.

Insect	**ν (Flagellomere)**	**ν**
Periplaneta americana	0.468±0.040	-0.417±0.155 **(**membrane)
Vanessa cardui	0.228±0.026	-0.296±0.091 (edge)
Manduca sexta	0.171±0.031	+0.216±0.094 (membrane)

An average Poisson's ratio for a flagellomere of *P. americana* was close to ½, $\nu_{PA-F} = 0.468 \pm 0.040$, suggesting that the antenna behaves as an incompressible material (Table 1). Having given its cross-sectional morphology, we conclude that the antennal interior occupied by blood, nerves, and tracheae effectively supports the applied load, distributing it over the entire cross-section. Blood facilitates this load distribution by generating a counter pressure acting on the cuticular shell and creating a circumferential or hoop stress on the flagellomere. The flagellomeres of *V. cardui* at the middle of the antenna where the taper angle is small and of *M. sexta* had Poisson's ratios of $\nu_{VC-F} = 0.228 \pm 0.026$, and $\nu_{MS-F} = 0.17 \pm 0.031$, respectively. These values are much lower than ½ and hence the radial deformations of antennae of these insects are less influenced by the blood.

The radial deformation of connecting membranes of *P. americana* and flagellomere edges of *V. cardui* differed from that of *M. sexta* (Fig. 9). At these points, the antennae of *P. americana* and *V. cardui* expanded in diameter during elongation and Poisson's ratios had respective average values of $\nu_{PA-M} = -0.417 \pm 0.155$ and $\nu_{VC-M} = -0.296 \pm 0.091$.

However, the membrane connection of the antenna of *M. sexta* resulted in a Poisson's ratio of $\nu_{MS-M} = 0.216 \pm 0.094$, which does not suggest expansion like the other two types of antennae.

The materials with negative Poisson's ratios are known as auxetic materials[40]. In many cases, the organization of constituent structures of the material plays the most important role in setting up this auxetic feature [41]. As found in *P. americana* and *V. cardui*, membranous cuticle connecting flagellomeres is responsible for this auxetic feature and these characters fall in line with the existing classification of the materials expansion mechanisms [41], as explained schematically in Fig. 9.

The analysis of Poisson's ratios of three selected insect species sheds light on the remarkable richness in mechanical behavior of their antennae. The presence of blood seems critical for antennae. Antennae of American cockroaches are full of blood and show the J-type strain-adaptive mechanical response. One observes a gradual decrease of blood in butterfly antennae as one goes from high humidity, where antennae demonstrate the J-type strain-adaptive behavior and the blood is visible, to low humidity where antennae demonstrate the Hookean behavior and no blood is seen after antennal breakup. The absence of visible blood and the Hookean behavior of hawkmoth antennae follow the same trend. These results point to important coupling of the blood pressure and mechanical response of these multifunctional fibers.

The effect of blood pressure is first theoretically explained in the next section and then validated on artificial flagellomeres modeled by plastic tubes of circular cross-section filled with water that models blood.

4. Characteristic features of deformation of blood-filled flagellomeres

The hypothesis that blood acts to distribute the applied load over the antennal cuticular shell can be examined by employing solid mechanics and setting up a simple model considering a single flagellomere as a circular tube filled with an incompressible liquid. In this model, no blood flow through the antennal vessel and lumen are considered, but blood interaction with the cuticular wall is taken into account through generation of its pressure. There are two scenarios for antennal loading.

In the first scenario, when the antenna is deformed, blood volume in the antenna is conserved. This scenario is applicable for description of antennal deformation when the insect lashes it during fighting or bends and pulls it during grooming or extraction from the old cuticle while molting (Fig. 6a–c). In the first approximation, as the pulling stroke might be much shorter than the frequency of the pulsatile organ (25–35 beats per min [28, 33]) one can assume that the blood amount in the antenna is conserved while the antennal shell deforms.

In the second scenario, the blood volume is not conserved. This scenario describes inflation or contraction of the antenna due to blood pumping, resulting in increase or decrease of the blood pressure, respectively (Fig. 6 d–f). The bending and straightening of the cockroach antenna due to the influence of blood pressure was observed in a cockroach restrained in a paper envelope with the antennae allowed to move freely. The cockroach antenna was allowed to move freely within the confines of two glass slides with an air gap between them. No external force was used to prompt the insect to move its antennae. A series of pictures in (Fig. 6 g–i) illustrate the insect's ability to bend and straighten the flagellum only with the increase or decrease of blood pressure. This scenario fits solid mechanics theory of pressurized tubes named after Gabriel Lamé [42, 43], Fig. 6 j).

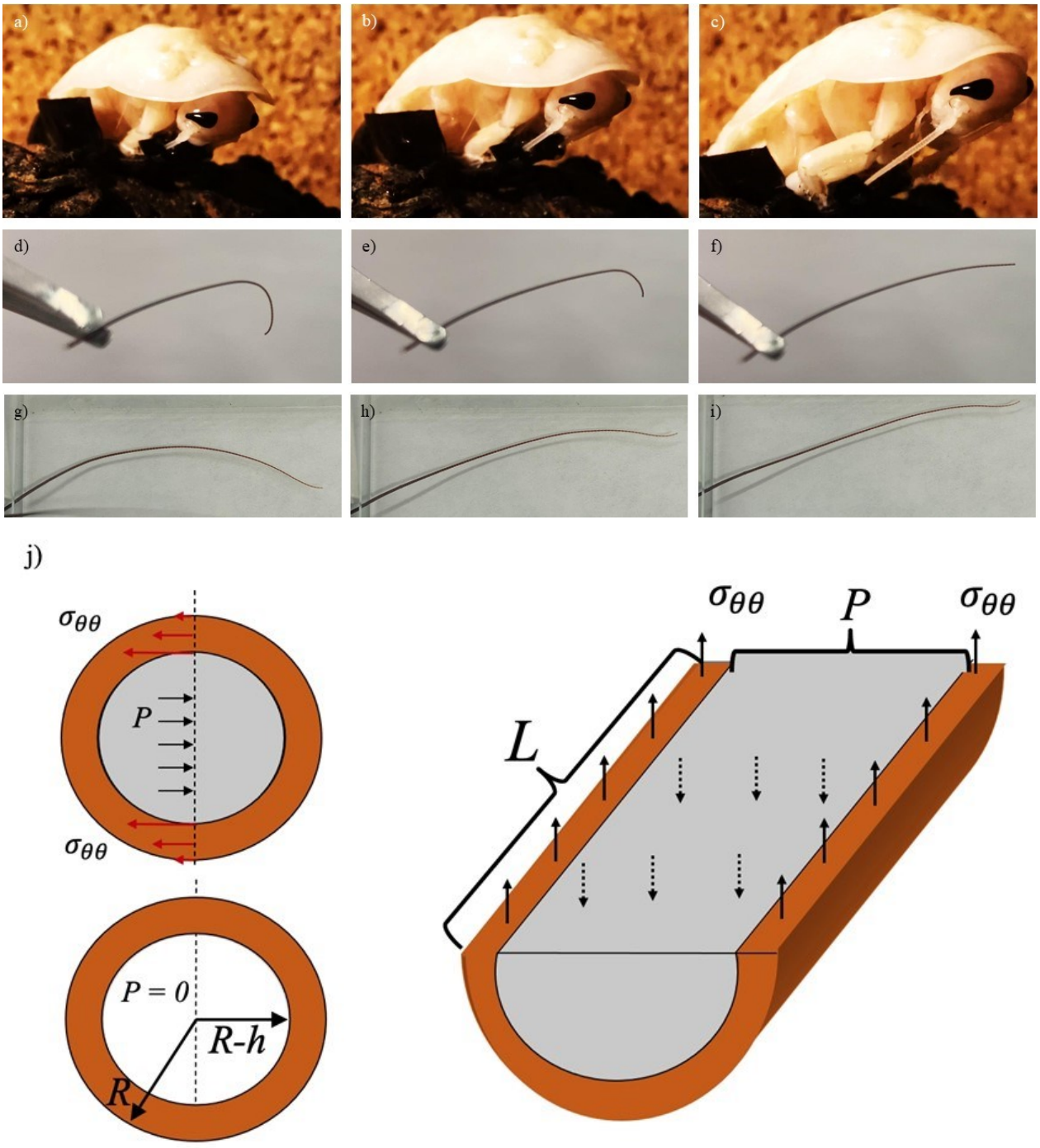

Figure 6. a–c) A series of images of the hissing cockroach (*Gromphadorhina oblongonata*) taken from a YouTube video[44]. During molting, the cockroach has to apply a strong force to pull out the antennae from their old encasing. d–f) By squeezing the base of an antenna just removed from *Periplaneta americana*, the curved antennal tip can be straightened. g–i) The bending and straightening of the cockroach antenna was observed in a live insect when a cockroach restrained in a paper envelope was allowed to move the antenna freely between two glass slides with an air gap between them. j) A flagellomere is modeled as

a circular tube of external radius R_2 and internal radius R_1 and length L filled with an incompressible liquid shown in grey. A flagellomere cross-section and longitudinal section illustrating the free body diagram for the zero-external-force scenario when the internal pressure P is counterbalanced by the hoop stress in the cuticle. In an empty flagellomere, blood pressure is absent; hence, no hoop stress is developed when the flagellomere is stretched/compressed longitudinally. The pressure $P = P_{blood} - P_{atm}$ is measured relative to atmospheric pressure P_{atm}; therefore, the external pressure on the wall is zero, $P = P_{atm} - P_{atm} = 0$.

4.1. Liquid-filled tube with sealed ends: problem formulation

To evaluate stresses in the tube filled with a liquid, we apply Hooke's law for the tube's material, using the compression modulus λ and shear modulus G related to Young's modulus E and Poisson's ratio ν as

$$G = \frac{E}{2(1+\nu)} \quad , \qquad \lambda = -\frac{E}{3(-1+2\nu)}. \tag{7}$$

In a cylindrical system of coordinates (z, r, θ), Hooke's law relating the stresses and strains is written as

$$\sigma_{rr} = (\lambda + 2G)\epsilon_{rr} + \lambda(\epsilon_{\theta\theta} + \epsilon_{zz}) \tag{8}$$
$$\sigma_{\theta\theta} = (\lambda + 2G)\epsilon_{\theta\theta} + \lambda(\epsilon_{rr} + \epsilon_{zz}) \tag{9}$$
$$\sigma_{zz} = (\lambda + 2G)\epsilon_{zz} + \lambda(\epsilon_{\theta\theta} + \epsilon_{rr}) \tag{10}$$

The radial and hoop strains are

$$\epsilon_{rr} = \frac{du}{dr}, \qquad \epsilon_{\theta\theta} = \frac{u}{r}, \tag{11}$$

where u is the radial displacement of the material particles. Thus, after deformation, the internal radius of the tube becomes $R_1 + u(R_1)$ and the external radius of the tube becomes $R_2 + u(R_2)$. The stress balance in the radial direction for the tube wall is written as

$$\frac{d\sigma_{rr}}{dr} + \frac{1}{r}(\sigma_{rr} - \sigma_{\theta\theta}) = 0. \tag{12}$$

And the radial stress must satisfy the following boundary conditions

$$\sigma_{rr}(R_1) = -P \quad at \quad r = R_1, \tag{13}$$

$$\sigma_{rr}(R_2) = 0 \quad at \quad r = R_2. \tag{14}$$

The sign in (13) follows the convention that positive pressure corresponds to compression of the fluid and negative pressure corresponds to its stretching. In solid mechanics, positive stress corresponds to tension and negative to compression. Therefore, when pressure P is negative, $P < 0$, the right hand side in eq. (13) is positive; hence, the radial stress is positive, resulting in tension. And vice versa, when the applied pressure is positive, the right hand side in eq. (13) is negative, resulting in compression of the tube wall.

4.2. Antennal deformation by applying non-zero-external-force (NZF)

In this case, external force F is applied to the ends of the antenna, and each flagellomere experiences the action of the same force. For evaluation of the radial stress in (8), we have to relate the z-strain, ϵ_{zz} , to the radial and hoop strains. To find this relation, we assume that the liquid in the core of the tube wets the walls and hence when the tube deforms, the liquid moves accordingly not forming bubbles. At the loads of interest, the liquid can be considered incompressible; therefore; we can use the continuity condition for the liquid column of length L when it is stretched to $L + \Delta L$ and its radius changes from R_1 to $R_1 + \Delta R_1$. When the tube ends are firmly sealed and the volume of the liquid remains unchanged, and assuming the tube deformations are small, $\Delta R_1 \ll R_1$, $\Delta L << L$, we write the condition of the volume conservation as

$$2\pi R_1 \Delta R_1 L + \pi R_1^2 \Delta L = 0. \tag{15}$$

This equation is rewritten in terms of displacement $u(R_1)$ of the internal wall of the tube as

$$\frac{2\Delta R_1}{R_1} + \frac{\Delta L}{L} = 0, \quad or \quad \frac{2u(R_1)}{R_1} + \frac{\Delta L}{L} = 0 \tag{16}$$

Introducing the z-strain as $\epsilon_{zz} = \frac{\Delta L}{L}$, we have from (11):

$$\epsilon_{zz} = -2\epsilon_{\theta\theta} = -\frac{2u(R_1)}{R_1}. \tag{17}$$

This equation shows that the z-strain does not depend on the radial coordinate r in the tube wall; i.e., each radial cross-section of the tube is stretched evenly. This equation reveals that positive displacement $u(R_1) > 0$ (i.e., tube expansion) results in negative z-strain ϵ_{zz} (i.e., contraction of tube length). And vice versa, negative displacement $u(R_1 < 0)$, results in positive z-strain ϵ_{zz} (i.e., extension of tube length).

Finally, to relate the pressure P in the liquid-filled tube with the applied tensile force F, we use the force balance equation:

$$F = -\pi R_1^2 P + (\pi R_2^2 - \pi R_1^2)\sigma_{zz} \tag{18}$$

Equation (17) allows one to express axial strain in terms of the radial displacement u and hence Hooke's laws (8)-(10) allow expression of the radial stress σ_{rr} in terms of the radial displacement. Then, eq. (18) defines the generated pressure. Hence, the boundary value problem (8)-(14) and (17)-(18) is closed.

4.3. Zero-external-force (ZF) scenario of antennal inflation/contraction

The model that we proposed, (8)-(14) and (17)-(18), is designed to describe the tensile experiments, assuming that the insect antennae are sealed tubes. It does not allow description of the characteristic features of antennal deformation when the insect increases or decreases blood pressure using its pulsatile organ. In that case, equations (15)-(18) cannot be applied because blood

volume is not conserved; the insect either pumps more blood into the antennae or draws it out on demand. Thus, the pressure generated by the pulsatile organ becomes the driving parameter. On the other hand, the total force on the antenna of a live insect is zero; hence, we have to replace (18) with

$$0 = -\pi R_1^2 P + (\pi R_2^2 - \pi R_1^2)\sigma_{zz}. \quad (19)$$

from which the axial stress is obtained as

$$\sigma_{zz} = \pi R_1^2 P/(\pi R_2^2 - \pi R_1^2). \quad (20)$$

The problem (8)-(14) and (20) is the classical Lamé problem of solid mechanics [42, 43]. The axial stress is obtained from (20) and Hooke's law (10) as $\pi R_1^2 P/(\pi R_2^2 - \pi R_1^2) = (\lambda + 2G)\epsilon_{zz} + \lambda(\epsilon_{\theta\theta} + \epsilon_{rr})$ or

$$\epsilon_{zz} = \frac{\pi R_1^2 P}{(\pi R_2^2 - \pi R_1^2)(\lambda + 2G)} - \frac{\lambda}{(\lambda + 2G)}(\epsilon_{\theta\theta} + \epsilon_{rr}). \quad (21)$$

And, therefore, (15)-(18) and (20)-(21) can be solved analytically to obtain the stresses and strains in the antenna.

4.4. Results of modeling

Table 2. Stresses, strains and the constants c_1 and $c_2$defining radial displacement $u(r) = c_1 r + c_2/r$ for zero force and non-aero force cases.

Parameter	Zero Force Case	Non-Zero Force Case
c_1	$-\frac{P(1+\nu)(-1+2\nu)R_1^2}{E(-2+\nu)(R_1^2 - R_2^2)}$	$-\frac{P(1+\nu)((-3+6\nu)R_1^2 - 2(1+\nu)R_2^2)}{3E(-1+2\nu)(R_1^2 - R_2^2)}$
c_2	$\frac{P(1+\nu)R_1^2 R_2^2}{E(-R_1^2 + R_2^2)}$	$\frac{P(1+\nu)R_1^2 R_2^2}{E(-R_1^2 + R_2^2)}$
ϵ_{rr}	$-\frac{P(1+\nu)R_1^2(r^2(-1+2\nu) - (-2+\nu)R_2^2)}{Er^2(-2+\nu)(R_1^2 - R_2^2)}$	$-\frac{P(1+\nu)(-2r^2(1+\nu)R_2^2 + 3(-1+2\nu)R_1^2(r^2 - R_2^2))}{3Er^2(-1+2\nu)(R_1^2 - R_2^2)}$
$\epsilon_{\theta\theta}$	$-\frac{P(1+\nu)R_1^2(r^2(-1+2\nu) + (-2+\nu)R_2^2)}{Er^2(-2+\nu)(R_1^2 - R_2^2)}$	$-\frac{P(1+\nu)(-2r^2(1+\nu)R_2^2 + 3(-1+2\nu)R_1^2(r^2 + R_2^2))}{3Er^2(-1+2\nu)(R_1^2 - R_2^2)}$
ϵ_{zz}	$-\frac{P(1+\nu)(-1+2\nu)R_1^2}{E(-2+\nu)(R_1^2 - R_2^2)}$	$\frac{2P(1+\nu)((-3+6\nu)R_1^2 + (-5+4\nu)R_2^2)}{3E(-1+2\nu)(R_1^2 - R_2^2)}$

σ_{rr}	$\frac{PR_1^2(-r^2+R_2^2)}{r^2(R_1^2-R_2^2)}$	$\frac{PR_1^2(-r^2+R_2^2)}{r^2(R_1^2-R_2^2)}$
$\sigma_{\theta\theta}$	$-\frac{PR_1^2(r^2+R_2^2)}{r^2(R_1^2-R_2^2)}$	$-\frac{PR_1^2(r^2+R_2^2)}{r^2(R_1^2-R_2^2)}$
σ_{zz}	$-\frac{PR_1^2}{R_1^2-R_2^2}$	$\frac{2P((-1+2\nu)R_1^2+(-2+\nu)R_2^2)}{(-1+2\nu)(R_1^2-R_2^2)}$
P	P	$-F(1-2\nu)[\pi(3(1-2\nu)R_1^2+2(2-\nu)R_2^2))]^{-1}$

Following the approach outlined in **Supplementary Material**, we obtained solutions to these two models and the resulting formulae are summarized in **Table 2**. Using these formulae, we can fully analyze these two scenarios of flagellomere loading.

The stress distribution through the thickness of flagellomere cuticle is shown as a heat map (Fig. 7a–d). The stresses correspond to the same axial strain $\epsilon_{\mathrm{zz}} = 0.01$. For both scenarios, the radial and hoop stresses change as we move through the tube thickness from the internal wall where the magnitude of these stresses is greatest, to the external wall where it is smallest. The striking difference between the zero-force and non-zero-force cases is the direction of compression-extension. For example, in the zero-force case, the radial stress is always negative, implying compression of the cuticular wall when the antenna is inflated by pressurizing the blood. The hoop stress in this case is tensile, implying that flagellomeres are stretched circumferentially when the antenna in inflated with blood. In contrast, when external force is applied to stretch the antenna, flagellomeres are subjected to radial tensile stress: the generated negative pressure of the blood pulls the cuticle inward toward the center, causing radial tension in the cuticle. Simultaneously, the flagellomeres are subjected to the compressive hoop stress, forcing them to contract in the circumferential direction.

In Fig. 7e, f, we plot the dependence of dimensionless pressure on the axial strain ϵ_{zz}. For both scenarios, this dependence is always linear, suggesting that blood works hand in hand with the cuticle to distribute the applied load. However, there is a striking difference between the zero-force and non-zero-force scenarios of flagellomere loading.

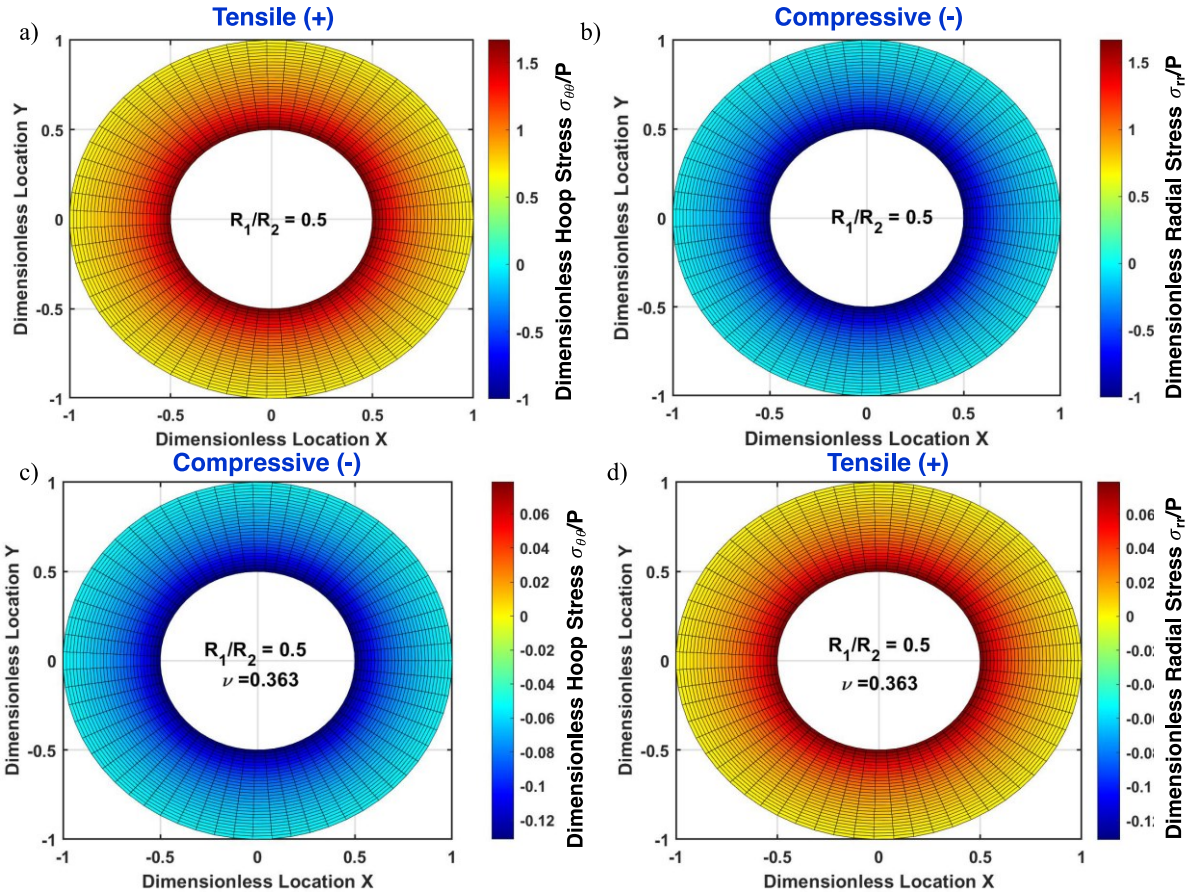
a)
Tensile (+)
R_1/R_2 = 0.5
Dimensionless Location Y
Dimensionless Location X
Dimensionless Hoop Stress $\sigma_{\theta\theta}/P$
b)
Compressive (-)
R_1/R_2 = 0.5
Dimensionless Location Y
Dimensionless Location X
Dimensionless Radial Stress σ_{rr}/P
c)
Compressive (-)
R_1/R_2 = 0.5
ν =0.363
Dimensionless Location Y
Dimensionless Location X
Dimensionless Hoop Stress $\sigma_{\theta\theta}/P$
d)
Tensile (+)
R_1/R_2 = 0.5
ν =0.363
Dimensionless Location Y
Dimensionless Location X
Dimensionless Radial Stress σ_{rr}/P

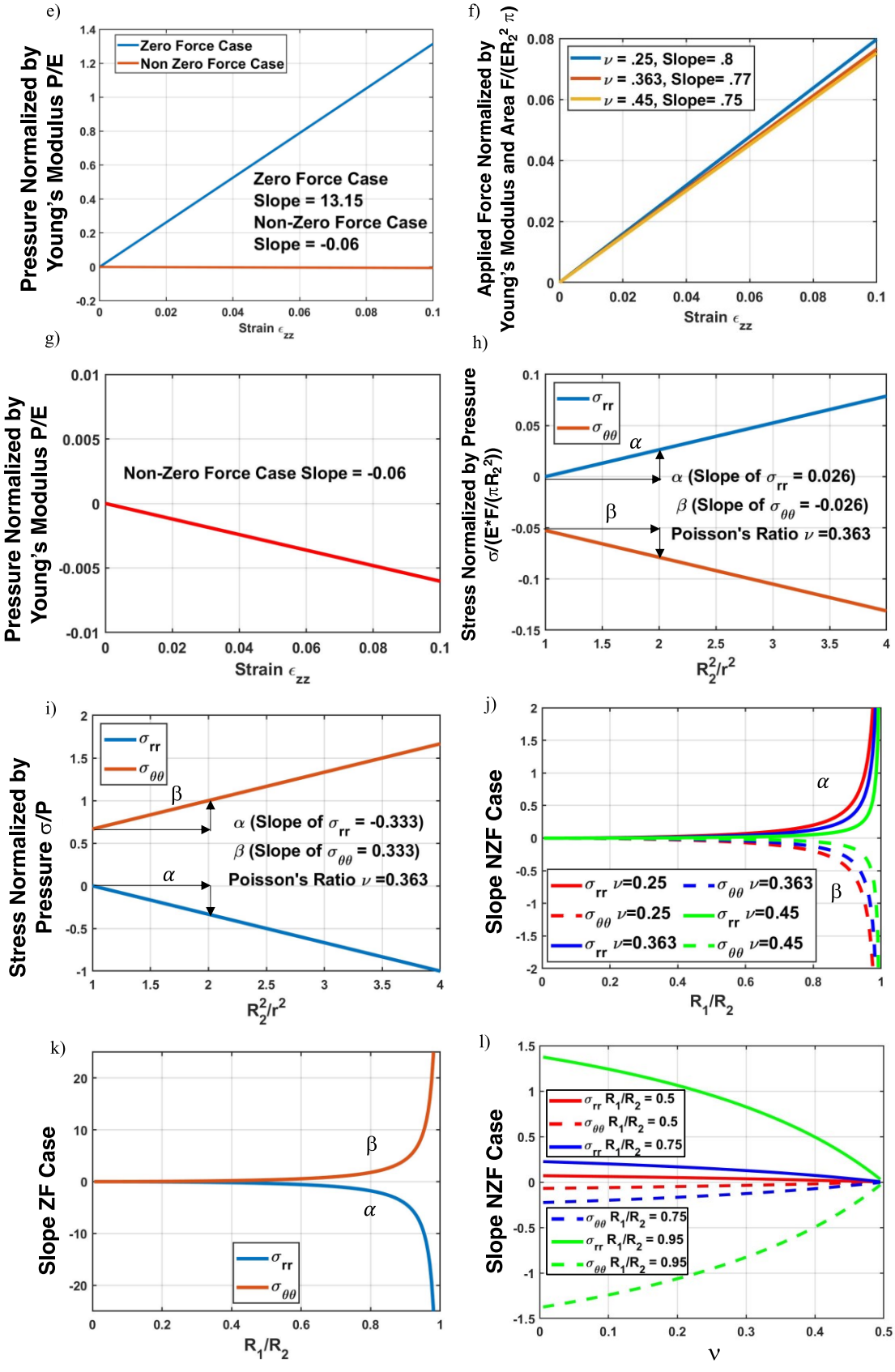
e)
Pressure Normalized by Young's Modulus P/E
Zero Force Case
Non Zero Force Case
Zero Force Case
Slope = 13.15
Non-Zero Force Case
Slope = -0.06
Strain ϵ_{zz}
f)
Applied Force Normalized by Young's Modulus and Area F/(ER$_2^2$ π)
ν = .25, Slope= .8
ν = .363, Slope= .77
ν = .45, Slope= .75
Strain ϵ_{zz}
g)
Pressure Normalized by Young's Modulus P/E
Non-Zero Force Case Slope = -0.06
Strain ϵ_{zz}
h)
Stress Normalized by Pressure σ/(E*F/(πR$_2^2$))
σ_{rr}
$\sigma_{\theta\theta}$
α
α (Slope of σ_{rr} = 0.026)
β (Slope of $\sigma_{\theta\theta}$ = -0.026)
β
Poisson's Ratio ν =0.363
R$_2^2$/r^2
i)
Stress Normalized by Pressure σ/P
σ_{rr}
$\sigma_{\theta\theta}$
β
α (Slope of σ_{rr} = -0.333)
β (Slope of $\sigma_{\theta\theta}$ = 0.333)
α
Poisson's Ratio ν =0.363
R$_2^2$/r^2
j)
Slope NZF Case
α
σ_{rr} ν=0.25
$\sigma_{\theta\theta}$ ν=0.363
$\sigma_{\theta\theta}$ ν=0.25
σ_{rr} ν=0.45
σ_{rr} ν=0.363
$\sigma_{\theta\theta}$ ν=0.45
β
R$_1$/R$_2$
k)
Slope ZF Case
β
α
σ_{rr}
$\sigma_{\theta\theta}$
R$_1$/R$_2$
l)
Slope NZF Case
σ_{rr} R$_1$/R$_2$ = 0.5
$\sigma_{\theta\theta}$ R$_1$/R$_2$ = 0.5
σ_{rr} R$_1$/R$_2$ = 0.75
$\sigma_{\theta\theta}$ R$_1$/R$_2$ = 0.75
σ_{rr} R$_1$/R$_2$ = 0.95
$\sigma_{\theta\theta}$ R$_1$/R$_2$ = 0.95
ν

Figure 7. a) Heat map for the hoop stress in a zero-external-force case normalized by pressure based on axial strain equal to ϵ_{zz} =0.01. b) Heat map for radial stress in a zero-external-force case normalized by pressure based on axial strain equal to $\epsilon_{zz} = 0.01$. c) Radial stress for a non-zero-external-force case. d) Hoop stress in a non-zero-external-force case normalized by the axial force divided by area. In Figs. 7e–l, the left column corresponds to the zero-external-force case, and the right column corresponds to the non-zero-external-force case. e) Pressure normalized by Young's modulus versus axial strain. Slope of the line depends on Poisson's ratio. f) Applied force normalized by Young's modulus and area for different Poisson's ratios. g) Zoomed in plot of Fig. 7g showing the slight slope of the non-zero-external force case. h) Lamé lines for the zero-external-force case. i) Lamé lines for the non-zero-external-force case. j) Slope of the Lamé lines for the zero-external-force case for different Poisson's ratios as a function of the ratio $R_1/\ R_2$. k) Slope of the Lamé lines for non-zero-external-force case for different Poisson's ratios as a function of the ratio $R_1/\ R_2$. l) Slope of the Lamé lines for non-zero-external-force case for different ratios $R_1/\ R_2$as a function of Poisson's ratio.

Lamé plots

The radial and hoop stresses depend on the radial coordinate r as $\sigma_{rr}, \sigma_{\theta\theta} \propto 1/r^2$. Therefore, the analysis of these stresses on physical parameters is convenient to perform using the so-called Lamé plot (Fig. 7h–i). This plot shows the normalized radial or hoop stresses as functions of the ratio R_1^2/r^2. The slopes of these lines depend on the ratio of internal to external radii of the tube and on the Poisson's ratio (Fig. 7j–l).

The Lamé plots (Fig. 7h–i) distinguish the loading scenario. While the radial and hoop stresses always have opposite signs and slopes, their directions for the zero-force and non-zero-force cases are opposite. For example, in the zero-force case, when the insect extends the antennae by pressurizing the blood, the radial stress is negative (compression). In the non-zero-force case, the applied tensile force results in the positive radial stress causing radial extension of the flagellomeres.

Effect of cuticular properties on Lamé plots

The slopes of the Lamé plots significantly depend on the thickness of flagellomere cuticle (Fig. 7j, k). The magnitudes of slopes on the Lamé plots increase as cuticle thickness decreases. Yet, the slopes do not depend on Young's modulus of the flagellomere material, but significantly depend on Poisson's ratio (Fig. 7l). As Poisson's ratio increases and the material tends to behave like a rubber, the slopes of the Lamé plots for the force-driven deformation of antennae become smaller, implying that the blood and cuticle deform in unison. For Poisson's ratio $\nu = 1/2$, the blood pressure remains at the atmospheric level. Thus, the closer the cuticle to the rubber-like incompressible material, the less perturbation that occurs when the insect stretches its antennae.

As this analysis shows, blood pressure coupled with stresses in flagellomere cuticle and connecting membrane effectively distribute the external load and work in the insect's favor. To validate this model, we used a plastic tube filled with water and studied its stress-strain behavior.

5. Artificial flagellomeres

5.1. Tensile experiments on artificial flagellomeres

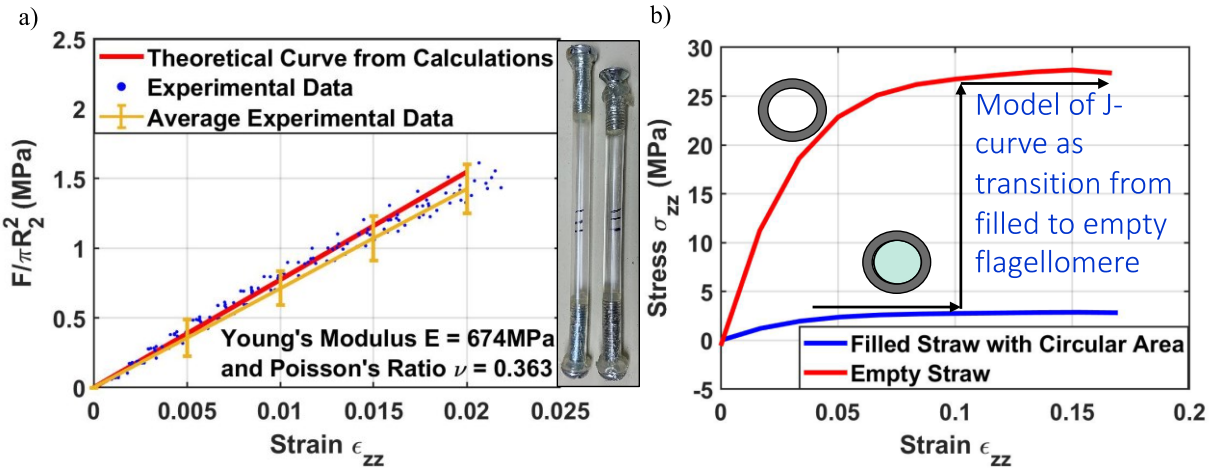

Figure 8. a) Comparison of experimental data with theory in terms of normalized tensile force versus axial strain for water-filled tubes. Force and strain were normalized to each sample's maximum force and its corresponding strain at that force. No adjustable parameters were used. The photograph shows plastic tubes, empty at the left and water-filled at the right, with screws at the ends supporting the cylindrical shape of the tubes during tensile experiments. b) Axial stress versus axial strain for empty and water-filled tubes. The stress is obtained by dividing the average force values by πR_2^2 for the water-filled tubes and by $\pi(R_2^2 - R_1^2)$ for the empty tubes. The J-curves of insect antennae could be explained by a transition from one type of mechanical behavior of the blood-filled antenna to the other type when the stress will be concentrated on the flagellomere cuticle. This transition is shown by the arrows.

Samples were loaded into the Instron machine so that the tops of the screws were beyond the edge of the clamp and the clamp pressed down on the length of the screw. Samples were extended for 10 cm at a rate of 50.8 mm/min.

Several phenomena were noticed during tensile testing. First, upon stretching, the cross-section of the water-filled tube was typically ovalized into a more ellipsoidal shape, even with the screw to initially support the cylindrical structure. On the other hand, the empty tubes remained round during tensile testing. Both tubes relaxed and shrank elastically after being released from the clamps.

Three times, a bubble was seen in the filled tubes that formed during tensile testing, typically at the top of the water-filled column, and was visible after testing in several of the samples. Bubbles possibly formed in more than a few water-filled samples but disappeared during the shrinking/relaxing process after being released from the clamps.

Generally, the water-filled tubes exhibited a lower maximum force and stress compared with the empty tubes. The water might help bear the load of the tensile force, thereby distributing the stress across the entire cross section of the tube compared with only the tube wall. Graphs support this idea by using a data set of all points normalized to the maximum force exerted on each sample and then averaged together (Fig. 8). From there, the average cross-sectional area was determined for each case. Because the water supports the force across the whole cross section, the area of filled tubes was calculated as $A_{filled} = \pi {R_2}^2$, where R_2 is the outer radius of the tube. The area of the empty tube was calculated as $A_{empty} = \pi({R_2}^2 - {R_1}^2)$, where R_1 is the inner radius of the tube.

From here, the average stress for each case was determined by multiplying the normalized force and the average force together and dividing by the average area in each case (Table 3).

Table 3. Parameters used in tensile testing of plastic straws.

	Filled Straw	Empty Straw
Average Max Force (N)	69.6±5.9	71.7±5.2
Strain at Max Force	0.17±0.02	0.17±0.03
Average Outer Radius (mm)	2.79±0.01	2.79±0.01
Average Inner Radius (mm)	2.63±0.01	2.63±0.01
Average Area (m^2)	2.44E-05±1.60E-7	2.59E-06±1.60E-7
Average Max Stress (MPa)	2.856±0.245	27.645±2.956

As observed in Fig. 8b, two types of mechanical behavior of the water-filled and empty tubes are distinguishable. The arrows in Fig. 8b illustrate an imaginable transition from one type of mechanical behavior of a blood-filled antenna to the other type. For example, this transition or manifestation of the J-type strain-adaptive behavior might occur when a predator stretches the prey's antenna until it is about to break. A trachea subject to the negative pressure of the blood should break first and a bubble could be released. Hence, the stress will be concentrated only on the flagellomere cuticle. In this schematic, the transition is sharp. Given the complexity of the tracheae, nerves, and hemocoel morphology, it is difficult to imagine that once an air bubble is released from the extended tracheae, it would immediately block the hemocoel at the same strain. Extra expansion probably would be required for the bubble to completely displace the blood from the antennal cross-section. Therefore, the J-curve is not sharp, but gradually changes as the strain increases.

We are not aware of any publications on characterization of tensile properties of the insect antenna as a whole. Characterization of mechanical properties of cuticle has been done mostly with the nano-indentation technique[45-47]. The most relevant data are provided by Dirks and Taylor who analyzed the tensile properties of one segment of the insect leg, the tibia, using cantilever beam tensile testing methods[48-50]. The measured breaking strength of the tibia was about two orders of magnitude larger than what we found for the antenna (Fig. 3b). Using our video-analysis, we noticed that before an antenna broke, the sensilla along the antenna tilted. Their angle with respect to the antennal axis changed when the antenna was pulled (Fig. S5). This angle remained almost the same from one flagellomere to the other at the given displacement, suggesting that the tensile stress was distributed evenly along the antenna before breakage. The antenna broke at the edge of a flagellomere and the crack appeared circumferential and clean. Thus, the low breaking strength of the antenna as a whole, compared with the greater breaking strength of the single leg segment (tibia), is explained by the low breaking stress of the connecting membrane at the contact point with a flagellomere.

6. Discussion

Despite the great diversity of insects and their antennae, the structural and functional organization of these appendages is based on a common basic trio of segments: scape, pedicel, and flagellum [1]. The muscles and joints in the scape and pedicel control 3D movement of antennae as rigid rods [7, 51]. The third component, the muscle-free flagellum, is divided into annular flagellomeres with stiff cuticle connected by folded membranes. A broad spectrum of antennal

morphology is based on structural modifications of the flagellum. These modifications mainly enlarge the antennal surface to accommodate additional sensilla. Thus, either the length of the antenna is increased or individual flagellomeres are enlarged by shape modification.

Long, filiform antennae, as in cockroaches and long-horned beetles, are typically used for tactile exploration of the environment. When touching objects or grooming antennae, these insects bend and sometimes loop their antennae. This force-driven deformation is distinguishable from deformations of the cantilevered antenna when no external forces are applied. For example, in resting cockroaches, the tips of their long antennae sag, but when these insects become active and start walking, the antennae are outstretched and straightened. We hypothesized that bending and flexing of the antenna can be controlled by blood pressure and that the blood would help bear the tensile or compressive load. Below, we provide examples of force-driven and blood-pressure-driven movements of antennae.

Blood-filled antennae create negative blood pressure when stretched and positive pressure when compressed

To remove debris, parasites, and pathogens from their long antennae, some insects pull them through specialized cuticular brushes on the legs or through the mouthparts to clean them [26]. By doing so, these insects apply a tensile force on their antennae. The tensile loading of antennae is seen in some male long-horned beetles fighting for females: when they lash one another with their antennae [18], the antennae are stretched by the beetle receiving the lashing.

When the antenna is subjected to tensile force, $F > 0$, the relative pressure in the lumen becomes negative (formula at bottom of Table 2), that is, the pressure in the blood drops below atmospheric pressure, resulting in contraction of the cuticular shell. Thus, the sign of pressure does not correspond to the sign of the axial stress developed in the cuticle. For example, during the pulling stroke on the antenna (Fig. 6 a–c), the cockroach applies positive tensile force, resulting in negative blood pressure relative to ambient pressure. And vice-versa, when the insect taps the antenna over a surface, compressing it, blood pressure in the lumen increases relative to ambient pressure.

Because membranes connecting flagellomeres are prone to unfolding and stretching, the blood pressure counteracts the unfolding. Therefore, blood pressure in the antennae effectively reacts to oppose membrane stretching and, hence, antenna extension.

Thus, having blood in the lumen, which opposes membrane unfolding, makes the insect antenna sturdier. As illustrated for *P. americana* and *V. cardui*, the shapes of folded antennal membranes can be complex. The simplest shape observed in *P. americana* looks like an axisymmetric collar obtained by rotating a 2D circular arc about the antennal axis. When the antenna is subjected to tensile force, $F > 0$, and the arc ends of the connecting chord attached to the flagellomeres are moved apart forcing the membrane to flatten, the negative blood pressure pulls it back to preserve the original configuration (Fig. 5g). The same mechanism works with the more complex shape of the membrane of *V. cardui* (Fig. 5d). The membrane, however, is folded on itself like a tilted V, providing stronger resistance to unfolding. In both cases, the blood pressure works to resist unfolding.

Tactile exploration of the environment by antennae typically involves tapping or touching of objects [10, 11]. When an insect explores an object with its antennae, the mechanical reaction force at the point of antennal contact with the object acts to compress each antenna along its axis, $F < 0$. According to our model, blood pressure in the lumen increases above atmospheric pressure.

Again, the blood pressure acts against folding the connecting membranes inward as the flagellomeres come together. Having this natural design of blood-filled antennae helps the insect deform them during behaviors such as grooming or tapping, without the possibility of breaking these important appendages.

To outstretch antennae, the insect has to increase its blood pressure

In a zero-force scenario, inflation or contraction of antennae is caused by increase or decrease of blood pressure, provided that no external force is applied to the antennae. The sign of applied pressure corresponds to the sign of the axial stress developed in the cuticle. For example, to stretch antennae, blood pressure needs to increase with respect to ambient pressure. By doing so, the insect imposes a positive tensile stress on the cuticular shell, stretching the antennae. And vice-versa, by dropping blood pressure below atmospheric, the insect imposes a contractive z-stress on each flagellomere, forcing the antennae to shrink in the axial direction. In other words, positive P corresponds to positive σ_{zz} and negative P corresponds to negative σ_{zz}. These pressure changes help the insect maneuver its antennae on demand. Indeed, the connecting membranes react to these pressure variations in unison: when blood pressure increases, the connecting membranes are prone to unfold, forcing the flagellomeres to move away from one another. When the pressure decreases below atmospheric, it forces the membranes to fold inward toward the lumen and the flagellomeres are dragged together, contracting the antennae.

In *V. cardui*, the majority of the sensilla are on the flagellomeres of the club-like tip of the antenna. In the resting position, these distal flagellomeres are nested like a stack, thereby protecting many of the sensilla. As our video analyses show, the club can be actively stretched, which exposes the sensilla and allows them to receive sensory stimuli. Similarly, when the antennae of the cockroach are stretched, even slightly, the hair-like sensilla decrease their angle of tilt with respect to the surface. Any degree of stretching, therefore, would increase the mechanoreception of antennal deformations.

Even more illustrative of the pressure-driven fanning of flagellomeres are the lamellate antennae of beetles in the family Scarabaeidae. Some species of this family live in substrates such as excrement, where sensilla could easily become contaminated. In the resting state, the lamellae of the antennae are tightly packed together and spread apart only for flight. As shown for the cockchafer (*Melolontha melolontha*), the lamellae spread only when the antennal hearts increase blood pressure [52]; after elimination of these organs, the beetles can no longer spread the lamellae.

Several scenarios are possible for blood control in antennae. The blood pressure can be elevated by increasing the frequency and/or amplitude of the antennal hearts to minimize backflow of blood to the head. No valve could be identified that would stop the backflow at the antennal base where the antennal lumen merges with the lumen of the head capsule. Even if a valve is lacking, backflow from the antennae can be prevented by increasing the blood pressure at the base by pumping blood from the posterior of the body. Thus, the increased blood pressure at the antennal base should reduce the backflow from the antenna.

Effect of environment

Our comparative study of the structure and mechanical performance of antennae of the hawkmoth *M. sexta*, butterfly *V. cardui*, and cockroach *P. americana* shows that the three antennal types are quite different in appearance and behavior. A systematic analysis of tensile properties

reveals a range of unexpected tensile properties, expressed either as Hookean brittle fibers (*M. sexta* at 33–84% humidity and *V. cardui* at 33–37% humidity) or strain-adaptive fibers that stiffen when stretched (*V. cardui* at 55–60% humidity and *P. americana* at 22–77% humidity). The strain-adaptive behavior is manifested through the J-type stress-strain relationship. J-type curves had been associated only with soft tissues[37, 53]. The antennal cuticle is stiff [13, 54] and hence this J-type behavior was unexpected.

A qualitative comparison of the antennal mechanical properties of each species was linked to the morphological features by using videomicroscopy during tensile testing. By capturing the deformation and breakup of antennae, a theoretical and experimental analysis was conducted to understand how the physical makeup of each insect's antennae was tied to differences in their mechanical properties. This behavior significantly depends on the structure of the antennae and blood supply. Thus, *V. cardui* and *P. americana* have slender cylindrical flagellomeres in which the antennal vessels run along the lumen wall and the blood returns to the insect body through a somewhat open body cavity (hemocoel). The blood and cuticle should, therefore, effectively share the applied load. Experiments confirm this expectation for *P. americana* over a broad range of humidity (22–77%). However, the butterfly antennae show this J-type behavior only at high (> 55%) humidity. In both cases, the antennae break at the connecting membranes, and at the fractured end, a blood meniscus spans the lumen of the butterfly and cockroach antennae.

In contrast, the fractured antennal ends of *M. sexta* and *V. cardui* at low (33–37%) humidity, do not show a blood meniscus spanning the lumen. We found the same result for *M. sexta* at higher humidity (>60%). In hawkmoths, the blood was mostly concentrated in the chambers of the antennal pectination, each extension of which is separated from adjacent ones. Blood in the butterfly antennae was mostly concentrated at the lumen wall as a film. Therefore, the blood would not actively support the load and only the membranous cuticle would support it. As a result, the stress-strain curves of antennae of the hawkmoth and the butterfly resemble those of a cotton fiber, which is basically a hollow tube with a complex cross-section.

Based on these observations, we infer that the American cockroach keeps its antennal lumen filled with blood even at low humidity. The painted lady butterfly fails to keep the antennal lumen filled with blood at low humidity and the Carolina hawkmoth fails to do this at *all* humidity levels. As a result, the stress-strain curves of their antennae differ drastically from the J-type curves. It is not clear how this change in mechanical properties affects insect performance in the field at low humidity.

Evolutionary perspective

All true insects have flagellate antennae. However, the situation for the most ancient lineages of the phylogenetic tree of Hexapoda is different: two primitively wingless (apterygote) taxa, Collembola and Diplura, have antennae in which all their segments have intrinsic musculature [23]. This antennal condition is considered plesiomorphic not only in hexapods, but also in all mandibulate arthropods [55]. The origin of flagellate antennae with multiple rings (flagellomeres) but without intrinsic musculature might be explained by the conquest of the terrestrial habitat, where these appendages can be moved in all directions. In contrast, the ancestors of Collembola and Diplura live in soil, the transitional habitat between the aquatic and terrestrial habitats in the evolution of the ancestors of insects. In the narrow crevices of soil, flagellate antennae would not be functionally suitable.

Antennae are derived from segmented ancestral legs [4, 56]. Given their adaptive value, the behavioral, mechanical, and structural properties of antennae that we have presented probably evolved deep in the arthropod phylogeny. By extension, we suggest these properties of insect antennae also can be found in other leg-derived appendages (e.g., mouthparts, legs, cerci, and genitalia[56]) that retain the subdivided nature of rigid cuticle separated by membrane, with or without intrinsic muscles. For example, long filamentous cerci (e.g., of silverfish) and subdivided tarsi of many insects, which lack intrinsic muscles, should behave like flagellomeres of antennae. Blood circulates through the various leg-derived appendages. Like antennae, some of these appendages of insects, such as thoracic legs of certain insects (Hemiptera and Orthoptera), also have autonomous pulsatile organs at their bases that provide the pressure to drive blood through the legs, although in legs the blood is guided by longitudinal diaphragms rather than by vessels [29]. Thus, as for antennae, blood would be expected to help support the tensile load of other leg-derived appendages, reducing the tensile stresses that would act on them.

Although well known as flexible sensory appendages, antennae are perhaps not fully appreciated for their ability to stretch. Conventionally, the membrane that connects segments and flagellomeres has been understood to unfold and flatten, providing extension of the appendage. We also show that this membranous cuticle and, to some extent the rigid cuticle, have the ability to stretch, providing even more extensibility. Through selection for increasingly elastic appendages, insects would have evolved this additional ability to resist breakage of their appendages during the bending and pulling that often occurs in courtship and mating[57], encounters with predators or competitors, or molting (Fig. 6a–c). Concomitant safeguarding of sensilla would also have been adaptive, the results of which are seen, for example, with the protected sensilla on the distal club of butterfly antennae.

7. Future Perspectives

Our findings demonstrate the rich structural and mechanical properties of insect antennae at multiple scales and suggest additional opportunities for examining the role of blood and cuticle in load distribution for any leg-derived appendages and the consequent implications for insect behavior and physiology. At the nanoscale, for example, we found that although Young's modulus sets up the magnitude of strain in the antennal cuticle, the stresses in the cuticle do not depend on Young's modulus but rather on Poisson's ratio, demonstrating the importance of the nano-scale organization and packing of alpha-chitin crystals and fibrils in the cuticle [53, 54, 58-61].

The principles we have outlined for antennae should apply generally to all serially homologous appendages of insects. Yet, the structural variety of these appendages and their associated functional diversity in roles such as feeding, mating, and flying are also associated with singular attributes that would make them attractive subjects for further investigation. All appendages are furnished with diverse sensilla specific to the functional needs of the particular extremity. We highlight one possible avenue of investigation, based on a sensory organ unique to antennae.

In addition to external mechanosensilla, each antenna harbors many proprioceptors in its base, which are arranged to form a complex, multifunctional sensory organ known as Johnston's organ [62]. It is highly sensitive to minute physical forces and serves a variety of functions such as controlling flight [7, 20, 63], detecting airborne sounds [16, 17, 64-66], and even sensing electrical fields [67].The possible connection between the vibratory properties of the antennae and

actuation of Johnston's organ, presents implications that should be of interest to sensory physiologists studying this extremely vibration-sensitive organ. We suggest that the role of blood pressure, particularly its coupling with cuticle deformation, in altering properties of antennal fibers deserves exploration. The antennae of hawkmoths, for example, vibrate at the wing-beat frequency[7]. As discussed earlier, this selected vibration frequency can be a result of blood pulsation in the insect head. When the moth rotates its body during flight, the antennae experience Coriolis (gyroscopic) and drag forces that perturb the background vibrations. These perturbations are converted to electrical signals by sensory units in Johnston's organ; without this input, flight stability is disrupted [7]. But the role of blood–cuticle coupling in detecting, monitoring, and controlling antennal motion in the mechanical loading on Johnston's organ during aerial maneuvers remains unexplored.

In mosquitoes, the antennae serve as hearing organs [16, 68, 69] with the ability to identify the direction of sound even when it arrives from the side. There is no direct evidence of deformation of the sensory units in Johnston's organ, but indirect estimates suggest surprisingly small, nanometer-scale, displacements leading to signal firing by the nerves [16, 69]. Blood flow through mosquito antennae [70] falls into our general schematic of blood–cuticle coupling, supporting the hypothesis that Johnston's organ is loaded through the blood–cuticle interaction, which helps in directional insect hearing.

These exciting ideas can be further developed to shed light on many other organismal appendicular features associated with blood–cuticle coupling. On the other hand, these findings put liquid-filled fibers [71-74] in a different category of fiber-based materials that offer unique multifunctionality [75, 76]. The walls of synthetic fibers are thick, and it is not easy to produce flagellomere-like fibers with thin walls [77, 78]. Therefore, to achieve the antenna-like functionality, a future direction would be to investigate a possible fabrication rout that could lead to a fiber with thin walls and a liquid core.

Acknowledgments

We thank Brittany Ellis in E. P. Benson's urban entomology laboratory for providing a steady supply of cockroaches. GD and KGK are partially supported by ORISE through the Air Force Civil Engineer Center at Tyndall Air Force Base. This work was partially supported by NSF grant IOS 2014664 to K. G. Kornev and P. H. Adler. The work of PHA was also partially supported by NIFA/USDA, under project number SC-1700527, with Technical Contribution No. 7035 of the Clemson University Experiment Station.

References

[1] R.F. Chapman, The Insects: Structure and Function, (2013).
[2] F.G. Barth, Mechanics to pre-process information for the fine tuning of mechanoreceptors, Journal of Comparative Physiology a-Neuroethology Sensory Neural and Behavioral Physiology 205(5) (2019) 661-686.
[3] J.A.C. Humphrey, F.G. Barth, Medium flow-sensing hairs: Biomechanics and models, in: J. Casas (Ed.), Advances in Insect Physiology: Insect Mechanics and Control, Elsevier Academic Press Inc, San Diego, 2007, pp. 1-80.
[4] A. Krishnan, S.P. Sane, Antennal Mechanosensors and Their Evolutionary Antecedents, in: R. Jurenka (Ed.), Advances in Insect Physiology, Vol 49, Academic Press Ltd-Elsevier Science Ltd, London, 2015, pp. 59-99.

[5] D. Schneider, Insect antennae, Annual Review of Entomology 9 (1964) 103-&.
[6] M. Gewecke, Antennae - another wind-sensetive receptor in Locusts Nature 225(5239) (1970) 1263-&.
[7] S.P. Sane, A. Dieudonne, M.A. Willis, T.L. Daniel, Antennal mechanosensors mediate flight control in moths, Science 315(5813) (2007) 863-866.
[8] S.P. Sane, Neurobiology and biomechanics of flight in miniature insects, Current Opinion in Neurobiology 41 (2016) 158-166.
[9] M. Gewecke, The antennae of insects as air-current sense organs and their relationship to the control of flight, in: L.B. Browne (Ed.), Experimental analysis of insect behaviour, Springer1974, pp. 100-113.
[10] J.M. Camhi, E.N. Johnson, High-frequency steering maneuvers mediated by tactile cues: Antennal wall-following by the cockroach, Journal of Experimental Biology 202(5) (1999) 631-643.
[11] J.M. Mongeau, A. Demir, C.J. Dallmann, K. Jayaram, N.J. Cowan, R.J. Full, Mechanical processing via passive dynamic properties of the cockroach antenna can facilitate control during rapid running, Journal of Experimental Biology 217(18) (2014) 3333-3345.
[12] J. Okada, Y. Kanamaru, Y. Toh, Mechanosensory control of antennal movement by the scapal hair plate in the American cockroach, Zool. Sci. 19(11) (2002) 1201-1210.
[13] H. Rajabi, A. Shafiei, A. Darvizeh, S.N. Gorb, V. Durr, J.H. Dirks, Both stiff and compliant: morphological and biomechanical adaptations of stick insect antennae for tactile exploration, Journal of the Royal Society Interface 15(144) (2018) 12.
[14] J. Okada, Y. Toh, Active tactile sensing for localization of objects by the cockroach antenna, Journal of Comparative Physiology a-Neuroethology Sensory Neural and Behavioral Physiology 192(7) (2006) 715-726.
[15] V. Durr, Y. Konig, R. Kittmann, The antennal motor system of the stick insect Carausius morosus: anatomy and antennal movement pattern during walking, Journal of Comparative Physiology a-Neuroethology Sensory Neural and Behavioral Physiology 187(2) (2001) 131-144.
[16] M.C. Gopfert, H. Briegel, D. Robert, Mosquito hearing: Sound-induced antennal vibrations in male and female *Aedes aegypti*, Journal of Experimental Biology 202(20) (1999) 2727-2738.
[17] H. Romer, Directional hearing in insects: biophysical, physiological and ecological challenges, Journal of Experimental Biology 223(14) (2020).
[18] L.M. Hanks, J.G. Millar, T.D. Paine, Mating behavior of the eucalyptus longhorned borer (Coleoptera: Cerambycidae) and the adaptive significance of long ''horns'', Journal of Insect Behavior 9(3) (1996) 383-393.
[19] E.M. Staudacher, M. Gebhardt, V. Durr, Antennal movements and mechanoreception: Neurobiology of active tactile sensors, in: S.J. Simpson (Ed.), Advances in Insect Physiology, Vol 322005, pp. 49-205.
[20] M. Gewecke, H.G. Heinzel, Aerodynamic and mechanical properties of the antennae as air-current sense organs in *Locusta Migratoria*. 1. Static characteristics, Journal of Comparative Physiology 139(4) (1980) 357-366.
[21] C. Loudon, J. Bustamante, D.W. Kellogg, Cricket antennae shorten when bending (Acheta domesticus L.), Frontiers in Physiology 5 (2014).
[22] B.D. Saltin, Y. Matsumura, A. Reid, J.F. Windmill, S.N. Gorb, J.C. Jackson, Material stiffness variation in mosquito antennae, Journal of the Royal Society Interface 16(154) (2019) 10.

[23] A.D. Imms, On the antennal musculature in insects and other arthropods, Q. J. Microsc. Sci. 81(322) (1939) 273-320.
[24] S.P. Sane, M.J. McHenry, The biomechanics of sensory organs, Integrative and Comparative Biology 49(6) (2009) I8-I23.
[25] M. Gewecke, Movement mechanism and joint receptors of antennae of *Locusta migratoria* L(Insects, Orthoptera), Zeitschrift Fur Morphologie Der Tiere 71(2) (1972) 128-149.
[26] K. Boroczky, A. Wada-Katsumataa, D. Batchelor, M. Zhukovskaya, C. Schal, Insects groom their antennae to enhance olfactory acuity, Proceedings of the National Academy of Sciences of the United States of America 110(9) (2013) 3615-3620.
[27] A. Frohlich, Z. Lu, Built to break: The antenna of a primitive insect, Petrobius brevistylis (Archaeognatha), Arthropod Structure & Development 42(2) (2013) 95-106.
[28] G. Pass, Antennal circulatory organs in Onychophora, Myriapoda and Hexapoda - functional morphology and evolutionary implications, Zoomorphology 110(3) (1991) 145-164.
[29] G. Pass, Accessory pulsatile organs: Evolutionary innovations in insects, Annual Review of Entomology 45 (2000) 495-518.
[30] S. Matus, G. Pass, Antennal circulatory organ of Apis mellifera L-(Hymenoptera : Apidae) and other Hymenoptera: functional morphology and phylogenetic aspects, International Journal of Insect Morphology & Embryology 28(1-2) (1999) 97-109.
[31] W. Hertel, H. Penzlin, Function and modulation of the antennal heart of Periplaneta Americana (L), Acta Biol. Hung. 43(1-4) (1992) 113-125.
[32] J.M. Suggs, T.H. Jones, S.C. Murphree, J.F. Hillyer, CCAP and FMRFamide-like peptides accelerate the contraction rate of the antennal accessory pulsatile organs (auxiliary hearts) of mosquitoes, Journal of Experimental Biology 219(15) (2016) 2388-2395.
[33] M.I. Pawlowa, Uber ampullenartige Blutcirculationsorgane im Kopfe verschiedener Orthopteren, ZOOLOGISCHER ANZEIGER 18 (1895) 7-13
[34] G. Pass, Gross and fine structure of the antennal circulatory organ in cockroaches (*Blattodea, Insecta*), Journal of Morphology 185(2) (1985) 255-268.
[35] A.L. Stockl, A. Kelber, Fuelling on the wing: sensory ecology of hawkmoth foraging, Journal of Comparative Physiology a-Neuroethology Sensory Neural and Behavioral Physiology 205(3) (2019) 399-413.
[36] J.F.V. Vincent, Structural Biomaterials, 3rd ed., Princeton University Presse, Princenton, NJ, 2012.
[37] M. Vatankhah-Varnosfaderani, W.F.M. Daniel, M.H. Everhart, A.A. Pandya, H.Y. Liang, K. Matyjaszewski, A.V. Dobrynin, S.S. Sheiko, Mimicking biological stress-strain behaviour with synthetic elastomers, Nature 549(7673) (2017) 497-501.
[38] K. Stamm, B.D. Saltin, J.H. Dirks, Biomechanics of insect cuticle: an interdisciplinary experimental challenge, Applied Physics a-Materials Science & Processing 127(5) (2021).
[39] H.R. Hepburn, H.D. Chandler, Material properties of Arthropod cuticles - arthrodial membranes, Journal of Comparative Physiology 109(2) (1976) 177-198.
[40] A. Alderson, K.L. Alderson, Auxetic materials, Proceedings of the Institution of Mechanical Engineers Part G-Journal of Aerospace Engineering 221(G4) (2007) 565-575.
[41] T.C. Lim, Analogies across auxetic models based on deformation mechanism, Physica Status Solidi-Rapid Research Letters 11(6) (2017).

[42] G. Lamé, Leçons Sur la Théorie Mathématique de l'Élasticité des Corps Solides, Bachelier, Paris, France, 1852.
[43] P. Schneider, R. Kienzler, Dimensioning of thick-walled spherical and cylindrical pressure vessels, Mathematics and Mechanics of Solids 25(7) (2020) 1405-1415.
[44] Crosser888, Hissing cockroach Gomphadorhina oblongonata molting, Youtube.com, 2016.
[45] J. Rivera, M.S. Hosseini, D. Restrepo, S. Murata, D. Vasile, D.Y. Parkinson, H.S. Barnard, A. Arakaki, P. Zavattieri, D. Kisailus, Toughening mechanisms of the elytra of the diabolical ironclad beetle, Nature 586(7830) (2020) 543-+.
[46] I. Kellersztein, S.R. Cohen, B. Bar-On, H.D. Wagner, The exoskeleton of scorpions' pincers: Structure and micro-mechanical properties, Acta Biomater. 94 (2019) 565-573.
[47] C.M. Hayot, S. Enders, A. Zera, J.A. Turner, Nanoindentation to quantify the effect of insect dimorphism on the mechanical properties of insect rubberlike cuticle, Journal of Materials Research 28(18) (2013) 2650-2659.
[48] J.H. Dirks, D. Taylor, Fracture toughness of locust cuticle, Journal of Experimental Biology 215(9) (2012) 1502-1508.
[49] E. Parle, H. Larmon, D. Taylor, Biomechanical factors in the adaptations of insect tibia cuticle, Plos One 11(8) (2016).
[50] E. Parle, S. Herbaj, F. Sheils, H. Larmon, D. Taylor, Buckling failures in insect exoskeletons, Bioinspiration & Biomimetics 11(1) (2016) 10.
[51] D. Natesan, N. Saxena, O. Ekeberg, S.P. Sane, Tuneable reflexes control antennal positioning in flying hawkmoths, Nature Communications 10 (2019).
[52] G. Pass, The anatomy and ultrastructure of the antennal circulatory organs in the cockchafer beetle *Melolontha - Melolontha L* (*Coleoptera, Scarabaeidae*), Zoomorphology 96(1-2) (1980) 77-89.
[53] J.F.V. Vincent, Structural Biomaterials, (2012).
[54] J.M. Gosline, Mechanical design of structural materials in animals, Princeton University Press, Princeton, NJ, 2018.
[55] G. Boxshall, D. Jaume, Antennules and antennae in the Crustacea, 2013.
[56] J. Kukalovapeck, The "Uniramia" do not exist - the ground plan of the Pterygota as revealed by Permian Diaphanopterodea from Russia (insecta,Paleodictyopteroidae), Canadian Journal of Zoology-Revue Canadienne De Zoologie 70(2) (1992) 236-255.
[57] P.H. Adler, C.R.L. Adler, Mating behavior and the evolutionary significance of mate guarding in 3 species of crane flies (Diptera: Tipulidae). Journal of Insect Behavior 4(5) (1991) 619-632.
[58] A.C. Neville, Biology of fibrous composites. Development beyond the cell membrane, Cambridge University Press, Cambridge, UK, 1993.
[59] D. Klocke, H. Schmitz, Water as a major modulator of the mechanical properties of insect cuticle, Acta Biomater. 7(7) (2011) 2935-2942.
[60] S.J. Ling, D.L. Kaplan, M.J. Buehler, Nanofibrils in nature and materials engineering, Nat. Rev. Mater. 3(4) (2018) 15.
[61] C.C. Li, S.N. Gorb, H. Rajabi, Cuticle sclerotization determines the difference between the elastic moduli of locust tibiae, Acta Biomater. 103 (2020) 189-195.
[62] L.H. Field, T. Matheson, Chordotonal organs of insects, in: P.D. Evans (Ed.), Advances in Insect Physiology, Vol 271998, pp. 1-228.

[63] H.G. Heinzel, M. Gewecke, Aerodynamic and mechanical properties of the antennae as air-current sense organs in *Locusta-Migratoria*. 2. Dynamic characteristics, Journal of Comparative Physiology a-Neuroethology Sensory Neural and Behavioral Physiology 161(5) (1987) 671-680.
[64] H.C. Bennet-Clark, Acoustics of insect song, Nature 234(5327) (1971) 255-+.
[65] H.C. Bennet-Clark, Size and scale effects as constraints in insect sound communication, Philosophical Transactions of the Royal Society of London Series B-Biological Sciences 353(1367) (1998) 407-419.
[66] T.R. Neil, M.W. Holderied, Sound production and hearing in insects, Advances in Insect Physiology 61 (2021) 101-139.
[67] U. Greggers, G. Koch, V. Schmidt, A. Durr, A. Floriou-Servou, D. Piepenbrock, M.C. Gopfert, R. Menzel, Reception and learning of electric fields in bees, Proceedings of the Royal Society B-Biological Sciences 280(1759) (2013).
[68] L.M. Roth, A study of mosquito behavior - an experimental laboratory study of the sexual behavior of *Aedes Aegypti (Linnaeus)*, American Midland Naturalist 40(2) (1948) 265-352.
[69] M.C. Gopfert, D. Robert, Nanometre-range acoustic sensitivity in male and female mosquitoes, Proceedings of the Royal Society B-Biological Sciences 267(1442) (2000) 453-457.
[70] S. Boppana, J.F. Hillyer, Hemolymph circulation in insect sensory appendages: functional mechanics of antennal accessory pulsatile organs (auxiliary hearts) in the mosquito Anopheles gambiae, Journal of Experimental Biology 217(17) (2014) 3006-3014.
[71] R. Hufenus, L. Gottardo, A.A. Leal, A. Zemp, K. Heutschi, P. Schuetz, V.R. Meyer, M. Heuberger, Melt-spun polymer fibers with liquid core exhibit enhanced mechanical damping, Materials & Design 110 (2016) 685-692.
[72] K. Jakubowski, W. Kerkemeyer, E. Perret, M. Heuberger, R. Hufenus, Liquid-core polymer optical fi bers for luminescent waveguide applications, Materials & Design 196 (2020).
[73] M. Naeimirad, A. Zadhoush, R. Kotek, R.E. Neisiany, S.N. Khorasani, S. Ramakrishna, Recent advances in core/shell bicomponent fibers and nanofibers: A review, Journal of Applied Polymer Science 135(21) (2018).
[74] A.J. Brown, N.A. Brunelli, K. Eum, F. Rashidi, J.R. Johnson, W.J. Koros, C.W. Jones, S. Nair, Interfacial microfluidic processing of metal-organic framework hollow fiber membranes, Science 345(6192) (2014) 72-75.
[75] R. Hufenus, Y.R. Yan, M. Dauner, T. Kikutani, Melt-Spun Fibers for Textile Applications, Materials 13(19) (2020).
[76] Y. Cheng, F.Y. Zheng, J. Lu, L.R. Shang, Z.Y. Xie, Y.J. Zhao, Y.P. Chen, Z.Z. Gu, Bioinspired Multicompartmental Microfibers from Microfluidics, Advanced Materials 26(30) (2014) 5184-5190.
[77] M. Heuberger, L. Gottardo, M. Dressler, R. Hufenus, Biphasic fluid oscillator with coaxial injection and upstream mass and momentum transfer, Microfluidics and Nanofluidics 19(3) (2015) 653-663.
[78] A.A. Leal, M. Naeimirad, L. Gottardo, P. Schuetz, A. Zadhoush, R. Hufenus, Microfluidic behavior in melt-spun hollow and liquid core fibers, International Journal of Polymeric Materials and Polymeric Biomaterials 65(9) (2016) 451-456.